ISA Transactions

Design of optimal cascade control approach for LFM of interconnected power system

--Manuscript Draft--

Manuscript Number:	ISATRANS-D-22-00394R2
Article Type:	Research article
Section/Category:	Design
Keywords:	Load frequency management Fractional order cascade controller Wild horse optimizer Interconnected power system Automatic generation control
Abstract:	In the present era, due to increasing power demand and complex power system structures having various load disturbances, a load frequency management (LFM) scheme is indispensable to provide uninterrupted power to consumers. This research deals with a fractional-order proportional derivative - (one + fractional order integrator) (FOPD-(1+FOI)) cascade controller as a novel control structure to ameliorate the performance of automatic generation control (AGC) for the LFM of interconnected power system (PS). The implementation of this controller is simple, and it connects the output of the FOPD controller to (1+FOI) controller, where area control error and power error are considered in the outer and inner feedback control loops, respectively. A maiden attempt of wild horse optimizer-assisted FOPD-(1+FOI) cascade controller for AGC of considered interconnected PS has been performed in this work. To benchmark the proposed control scheme, two areas reheat thermal PS with governor dead band and generation rate constraint nonlinearities are considered as the test bench. A vivid comparative analysis of six state-of-the-art control techniques is performed, and the results show the effectiveness of the proposed control scheme. Eigenvalues-based stability evaluation of considered interconnected PS in conjunction with the proposed controller is also performed. Finally, for the real power system implementation of the presented control scheme, a New England IEEE 39 test bus system is considered and analysed.

Response Sheet

Response to the suggestions and comments on **Manuscript No.**: **"ISATRANS-D-22-00394R2"** entitled "Design of optimal cascade control approach for LFM of interconnected power system" submitted to '*ISA Transactions'.*

Authors would like to thank honorable Editor-in-Chief (EIC), honorable Associate Editor (AE), and Reviewers for allowing us to incorporate the suggestions, thereby improving the quality of the paper. Most of the recommendations given by the reviewers are included in the currently revised manuscript. Suggestions and comments of reviewers are depicted in bold font style, and the reply is given in regular font style. The corrections in the manuscript have been depicted in red color text.

Reply to Reviewer #1:
The authors will like to thank the honorable reviewer for an extensive review of the paper and for the nice suggestions made to improve the quality of the article. The following are the response to the suggestions of the reviewer.

1. **I very much appreciate the authors' efforts to improve the quality of the work. The current version of the paper is much better than the previous one. However, there are still some issues. Below, please find a list of them.**

Reply: Authors are highly thankful to the honorable reviewer for the encouraging comments on the manuscript.

Abstract

2. **Very often the "*load demand uncertainties"* are called simply as load disturbances or briefly disturbances. Uncertainty is rather used in terms of metrological, model and parameter's properties.**

Reply: As per the valued suggestions of the honorable reviewer, authors have corrected the currently revised manuscript.

Review of the literature:

3. **The reader, I presume expects at this point at least the critical analysis of solutions of similar problems. The current version of the literature review unfortunately does not meet this expectation. It has a form of the set of short abstracts.**

Reply: As per the valued suggestions of the honorable reviewer, critical analysis has been highlighted at the end of the literature review section in the currently revised manuscript. Thanks for your suggestions; by including this, the quality of the introduction is enhanced and very useful for the author's future research work.

Subsection 1.3.

4. **Cit." *However, as per the best knowledge of the authors' results obtained in these works, have some space for enhancement while considering the time domain specifications*".**

I would like to mention that the parameters of the time domain are neither explicitly defined nor given in the previous section, which lists some of the known approaches.

Reply: As per the valued suggestions of the honorable reviewer, authors have corrected accordingly.

5. **Dynamic models. Fig. 1:**

Models of reheater and PS are linear. They are obtained for a fixed operating point, and therefore they are valid only in the near vicinity of the operating point. At least parameters of these models are depending on the current operation point.
The same applies for governor and turbine, where simply dead zone and limiter were introduced. However, this does not give an assumption to simulate the real behavior of the system by significant changes of the operating points or by turbine start-up or shutdown. This scheme does not allow to proper assessment of the proposed approach in stated above cases.
Please discuss this issue.

Reply: Respected reviewer, true linearized model is used for PS and reheater. The GDB and GRC-type nonlinearities are included to replicate the practical scenario. The considered literature for modeling is listed as follows:

1. N. Pathak and Z. Hu, "Hybrid-peak-area-based performance index criteria for AGC of multi-area power systems," *IEEE Transactions on Industrial Informatics*, vol. 15, no. 11, pp. 5792-5802, 2019.
2. N. Pathak, T. Bhatti, A. Verma, and I. Nasiruddin, "AGC of two area power system based on different power output control strategies of thermal power generation," *IEEE Transactions on Power Systems*, vol. 33, no. 2, pp. 2040-2052, 2017.
3. M. Ramesh, A. K. Yadav, and P. K. Pathak, "Intelligent adaptive LFC via power flow management of integrated standalone micro-grid system," *ISA transactions*, vol. 112, pp. 234-250, 2021.
4. Y. Arya, "ICA assisted FTIλDN controller for AGC performance enrichment of interconnected reheat thermal power systems," *Journal of Ambient Intelligence and Humanized Computing*, pp. 1-17, 2021.
5. E. Çelik, Öztürk, N., Arya, Y., & Ocak, C., "(1+ PD)-PID cascade controller design for performance betterment of load frequency control in diverse electric power systems " *Neural Computing and Applications*, pp. 1-24, 2021.
6. P. K. Pathak, A. K. Yadav, A. Shastri & P.A. Alvi, "BWOA assisted PIDF-(1+ I) controller for intelligent load frequency management of standalone micro-grid," *ISA Transactions*, pp. 1-15, 2022.
7. E. Çelik, "Performance analysis of SSA optimized fuzzy 1PD-PI controller on AGC of renewable energy assisted thermal and hydro-thermal power systems," *Journal of Ambient Intelligence and Humanized Computing*, pp. 1-20, 2022.

Moreover, large parametric variations in the considered plant's parameters are chosen to benchmark the robustness of the proposed control scheme (replicate the practical scenarios). Finally, real power system implementation via IEEE-39 test bus system is also performed to benchmark the controller performance. Respected reviewer, a vivid description of the two area power system's modeling is present in the currently revised manuscript.

6. Fig. 5: Please consider unifying the format of Figs. 5 and 6. Much better for analysis would be presenting Fig. 5 in the form as Fig. 6 i.e., as one chart instead of four separate charts.

Reply: Thank you very much for your observations. Respected reviewer, it is true that the format of Fig. 6 is much better for the analysis, but in the case of Fig. 5, the y-axis data and the pattern of convergence are in such a manner that they can not be considered as one chart (will not be clearly visible). Hence they are in four separate charts.

7. Please consider changing description given in paragraph below Fig. 6, to a simple table presenting obtained numerical results.

Reply: As per the valued suggestions of the honorable reviewer, authors have incorporated a separate table (Table 1) for a clear description.

8. Please cancel significant part of the text below Fig. 7. There are redundant data as in Tab. 1.

Reply: As per the valued suggestions of the honorable reviewer, a few redundant lines are removed and corrected accordingly.

9. The text in the right column above Tab. 1:
Cit.: "*While dealing with the error constants*…". Please clarify, what is a meaning of "*error constants*"?

Reply: Respected reviewer, error constants are clearly explained in the currently revised manuscript (Subsection 1.3).

10. Tables 1 and 2.
Consider using bold font to mark best results in each row.

Reply: As per the valued suggestions of the honorable reviewer, the obtained best results via the proposed LFM technique are now in the bold form in Tables 1, 2, and 3.

Reviewer #2:

I appreciate the authors effort in revising the manuscript and writing the response for my comments. All of my comments are addressed very well. I would like to appreciate the authors especially for the effort made in writing the response for the comments 2, 3, and 4, in which they have presented the convergence analysis,

computational costs, and motivation as compared to other complex controllers by providing suitable references. The revised manuscript is acceptable.

I recommend to accept and publish this paper without any further change.

Reply: Respected reviewer, authors are highly thankful for accepting the manuscript.

Reviewer #3:

The authors will like to thank the reviewer for an extensive review of the paper and for the nice suggestions made to improve the quality of the article. The following are the response to the suggestions of the reviewer.

1. **The corrections are done as per reviewer's instructions. Avoid honourable/respectful reviewer.**
Reply: Authors are highly thankful for your encouraging comment.

2. **Fractional Calculus is different from fractional controller. Basic difference author must know.**
Reply: Yes, reviewer, authors are agreed with your valuable observations.

3. **Many short forms are used. But all expansions are not mentioned. Put Nomenclature in the manuscript.**
Reply: As per the valued suggestions of the reviewer, a list of abbreviations is incorporated in the currently revised manuscript.

4. **Strong novelty of the proposed work must include in the Introduction section.**
Reply: Yes, reviewer, novelties are included in the introduction section in points form.

5. **Table 4 Eigen values, how impact your system?**
Reply: Reviewer, in order to perform the stability analysis of the proposed LFM scheme, an eigenvalues-based approach is implemented. The detailed eigenvalues show that all the poles are located in the left half of the s-plane, ensuring the system's stable operation.

Reviewer 5:
I appreciate the authors' efforts in this work, and the authors have revised the paper carefully, based on the comments from the reviewers. In my opinion, it can be accepted at this version.
Reply: Respected reviewer, authors are highly thankful for accepting the manuscript.

Authors would like to thank the honorable Editor-in-Chief for allowing us to incorporate the suggestions, thereby improving the quality of the paper. Almost all the suggestions of reviewers have been addressed, and hence it is hoped that the modified version of the paper meets the requirements for possible publication in *'ISA Transactions'*. However, the authors will be happy to incorporate if there are any further suggestions for improving the quality of the paper.

Highlights for Review

- Optimal cascade control for load frequency management
- WHO assisted FOPD-(1+FOI) cascade controller
- Load frequency management of interconnected power system

Design of optimal cascade control approach for LFM of interconnected power system

Article history:
Received xxxxx
Received in revised form xxxxx
Accepted xxxxx
Available online xxxxx

Keywords:
Load frequency management
Fractional order cascade controller
Wild horse optimizer
Interconnected power system
Automatic generation control

ABSTRACT

In the present era, due to increasing power demand and complex power system structures having various load disturbances, a load frequency management (LFM) scheme is indispensable to provide uninterrupted power to consumers. This research deals with a fractional-order proportional derivative - (one + fractional order integrator) (FOPD-(1+FOI)) cascade controller as a novel control structure to ameliorate the performance of automatic generation control (AGC) for the LFM of interconnected power system (PS). The implementation of this controller is simple, and it connects the output of the FOPD controller to (1+FOI) controller, where area control error and power error are considered in the outer and inner feedback control loops, respectively. A maiden attempt of wild horse optimizer-assisted FOPD-(1+FOI) cascade controller for AGC of considered interconnected PS has been performed in this work. To benchmark the proposed control scheme, two areas reheat thermal PS with governor dead band and generation rate constraint nonlinearities are considered as the test bench. A vivid comparative analysis of six state-of-the-art control techniques is performed, and the results show the effectiveness of the proposed control scheme. Eigenvalues-based stability evaluation of considered interconnected PS in conjunction with the proposed controller is also performed. Finally, for the real power system implementation of the presented control scheme, a New England IEEE 39 test bus system is considered and analysed.

Abbreviations

ABC	Artificial bee colony
ACO	Ant colony optimization
AGC	Automatic generation control
ANFIS	Adaptive neuro-fuzzy inference system
ANN	Artificial neural network control
BWOA	Black widow optimization algorithm
COA	Coyote optimization algorithm
DE	Differential evolution
DSA	Dragonfly search algorithm
FA	Firefly algorithm
FO	Fractional order
FOPID	Fractional order PID
GA	Genetic algorithm
GDB	Governor dead band
GOA	Grasshopper optimization algorithm
GRC	Generation rate constraint
GSA	Gravitational search algorithm
hBFOA	Hybrid bacterial foraging optimization algorithm
HHO	Haris hawk optimization
IAE	Integral of absolute error
ISE	Integral of squared error
ITAE	Integral of time multiplied absolute error
ITSE	Integral of time multiplied squared error
LFD	Levy flight distribution
LFM	Load frequency management
MBA	Mine blast algorithm
MGWO	Modified grey wolf optimization
MVO	Multi-verse optimization
OS	Overshoot
PDF	Proportional-derivative with filter
PI-PD	Proportional integral-Proportional derivative
PID	Proportional-integral-derivative
PS	Power system
PSO	Particle swarm optimization
QOHS	Quasi-oppositional harmony search
SBL	Stability boundary locus
SSA	Salp swarm algorithm
TSA	Tunicate swarm algorithm
US	Undershoot
WHO	Wild horse optimizer

1. Introduction

1.1 Background

Due to racing power demand in today's world, including PS size spurt, complexity, and interconnected PS network, it is a very challenging task to provide secure, uninterrupted, and stable power via proper power flow management [1]. The power demand is continuously fluctuating in nature, resulting in transient deviations in frequency and tie-line power flow of the entire PS [2-4]. Various control areas are connected to a PS network. From the electrical utility point of view, for stable and reliable operation, power generated in each control area must be equal to the power demands, and total losses occurred; as well as tie-line and deviation of frequency from reference should fall within permissible close to zero limits. To this end, noteworthy and rapid development has been seen in the LFM area because it is impossible to maintain the balance among demands-generations without supplementary control action [5, 6]. In real-time, AGC is the control action

that stabilizes the demand-generation balance and maintains the frequency deviations of the entire PS within permissible limits. In other words, LFM force the synchronous generator units to regulate their generations to meet the load demands. In view of the above-mentioned discussion, an enhanced and effective control scheme is an unavoidable requirement for the LFM of PSs. Moreover, for the purpose of engineering commissioning, the practical potential and suitability of an LFM control scheme in a real-time implementation is a much-needed feature [7-9].

1.2 Literature Review

From the comprehensive literature survey, it is pointed out that there are enormous highly cited works in the area of LFM present in the last few decades. Every article is endeavoring for further enhancement. In Ref. [2], PIDD2 controller based on the internal model control and worst-case plant selection scheme is proposed for the LFM of time-delayed interconnected PS. A novel performance index based on a hybrid peak area for the AGC of interconnected PS is briefed in [3]. In this, the authors have performed a comparative analysis of the proposed performance index with the existing indices. A fuzzy logic-based adaptive LFM of renewable energy shared standalone microgrid is demonstrated in [5]. In this, a fuzzy observer is used to extract the power from wind turbine generator, and an improved incremental conductance scheme is used to harvest maximum power from the solar. For the real power system implementation of the proposed control scheme, authors have considered a New England IEEE 39 test bus system. A fuzzy logic-based fractional variant of the PID controller is used to investigate the AGC performance of interconnected PS [7]. Few articles that are recently published employing PI/PID based controllers are (hBFOA-PSO) [10], BFOA [11], FA [12], lozi-map based chaotic algorithm [13], MGWO [14], ACO [15], QOHS [16], GA [17], DSA [18], DE [19], symbiotic organisms search [20], ABC [21], GWO tuned PI/PID controllers [22], and Jaya algorithm assisted PID with low pass filter [23]. To palliate control mechanism, other advanced control techniques based on H-infinity [24], sliding mode control [25], fractional calculus theory [26], model predictive control [27, 28], fuzzy logic approach [29], nonlinear disturbance observer [30], ANN [31], and ANFIS [32] are presented in the relevant field. A double-stage PI-(1+PD) controller is designed via a GOA scheme for the LFM of wind-ocean-based maritime PS in [33]. A comparative analysis among PID, PIDF, and PI-(1+PD) tuned via GA, PSO, FA, and GOA is performed, and the obtained results revealed the superior performance of the proposed controller. Design consideration of the cascade controller for the frequency control of multi-area PS based on COA is briefed in [34]. The simulation results revealed the proposed cascade PDF-PI controller's superior and robust dynamic performance under parametric uncertainties. The maximum frequency deviations under the worst condition are not exceeding 0.4% for the proposed control scheme. Online LFM in wind integrated PSs via modified jaya optimization is described in [35]. The performance assessment of SSA tuned intelligent fuzzy 1PD-PI controller for the AGC of renewable rich multi-area PS is presented in Ref. [36]. In this, author has designed a cascade control approach for the frequency control with the stability evaluation of the proposed technique. A frequency deviation mitigation technique via COA tuned fuzzy controller under wind integrated PS is briefed in [37]. A frequency control mechanism of distributed energy resources based on coordinated strategies is revealed in [38]. In this, small signal dynamic models for renewable energy sources are introduced in standalone microgrid. Design of active disturbance rejection based LFM of time delayed PS is demonstrated in [45]. Fraction order controller is designed for the AGC of multi area PS in Refs. [46, 47].

The PS works under various uncertainty conditions due to stochastic load demands, inherent nonlinearities, communication delays, and continuous variation in its structure. Though the intelligent algorithms tuned conventional controllers, as mentioned above, show good performance, their performance may greatly affect in regards to longer settling time and larger oscillations. Moreover, the output of the traditional controllers optimized for a specific point will worsen with changing operating conditions of the system. The fractional and cascade concept of controller design is much appreciated for its enhanced disturbance rejection capability before it is transmitted to other sections of the system and as underlined by researchers. A cascade control structure has the potential to provide enhanced performance to the traditional controller [39]. In this regard, MGWO tuned PI-PD cascade controller [14], BWOA tuned PIDF-(1+I) controller [40], bat algorithm optimized PD-PID cascade controller [41], DE based multi-stage PDF plus (1+PI) controller [42] are briefed for LFM of various PSs.

From the above-mentioned vivid literature review, the critical observations are; (1) the implementation of the metaheuristic approach on the fuzzy-logic, ANN and ANFIS, makes the system very complex, (2) designed controllers in the literature are just standard feedback control-based approach, and (3) there is always a scope to implement robust, advanced, and recently invented metaheuristic approach for the LFM of the power system.

1.3 Motivation and Contributions

The system responses of these cascade controllers are showing worth appreciating control effort in the area of interest. However, as per the best knowledge of the authors' results obtained in these works have some space for enhancement while considering the time domain specifications such as OS, US, rise time, and settling time, as well as error constants such as IAE, ITAE, ISE, and ITSE. The presented study revisits LFM by introducing a new factional and cascade controller named FOPD-(1+FOI), whose benchmarking is not yet investigated so far. In view

of the inspected literature, various nature-inspired optimizations are implemented in LFM studies for the purpose of proper gain tuning and to obtain the possible outcome from the controllers. WHO, a recently invented metaheuristic algorithm proposed by Iraj Naruei and Farshid Keynia (2021) [43] has proved its efficacy over GA, PSO, GWO, MVO, TSA, LFD, SSA, GSA, and HHO in various problems such as [43]; process synthesis and design, heat exchange design, two-reactor problem, tension/compression spring design, step-cone pully, three bar truss design, rolling-element bearing, and gas transmission compressor design, so it is considered for the LFM of the considered interconnected PS. A vivid comparative analysis of the proposed LFM controller design in terms of time-domain indices and error rates is performed with other metaheuristics like; GWO, MBA, MGWO, and recently invented BWOA [44], and other control structures like; FOPID, PI-PD, and PID. Moreover, a stability evaluation of the proposed LFM scheme is also performed in this work. For the stability evaluation, the fractional orders are approximated into their respective full-order terms via the SBL method [48]. In comparison with the existing literature, the significant contributions of the work are as follows:

1) Design of WHO tuned FOPD-(1+FOI) fractional cascade controller for LFM of two areas PS and its superiority has been established over designed FOPID, PI-PD, and PID controllers.
2) Performance assessment of WHO is verified over MBA, GWO, and BWOA concerning minimum fitness value, cost-effectiveness, and convergence rate.
3) Benchmarking of the proposed controller's robustness concerning parametric uncertainties and load disturbances.
4) Eigenvalues-based stability evaluation of the proposed LFM scheme.
5) For real power system validation, the proposed LFM technique is implemented on New England IEEE 39 test bus system.

The rest of the paper is documented as; Section 2 deals with the studied PS model, and Section 3 describes the vivid design consideration of the proposed controller. A vivid description of WHO is presented in Section 4, results and discussion with stability evaluation and real power system implementation are revealed in Section 5. The final concluding remark is given in Section 6.

2. Power System Model Under Investigation

A two-area interconnected reheat thermal PS is investigated and revealed in Fig. 1, and each PS control area has a load of 2000 MW. The reheat thermal PS with GDB and GRC has been comprehensively captivated in the AGC literature [2, 3] and [6, 8]. The generation speed is restricted due to the practical moderation of thermal and mechanical activities shown by GRC. On the other hand, GDB is a measure of continuous speed variation in which there is no deviation in the position of the valve. In order to conduct a real-time investigation on AGC in the presence of nonlinearities, GDB and GRC must be considered. In Fig. 1, the various components are as: area control error (ACE), governor regulation (R), frequency biasing (β), controller output (ΔP_c), turbine time constant (TC) (T_T), governor TC (T_G), reheater TC (T_r), reheater gain (K_r), change in load (ΔP_D), power error P_e, turbine power (ΔP_g), PS gain (K_{PS}), PS TC (T_{PS}) and area capacity ratio (α_{12}). Moreover, ΔF_i (change in frequency), $\Delta Ptie_{ij}$ (change in tie-line power), and T_{ij} (synchronizing coefficient). The detailed parameters of the considered two-area reheat thermal PS are provided in Appendix.

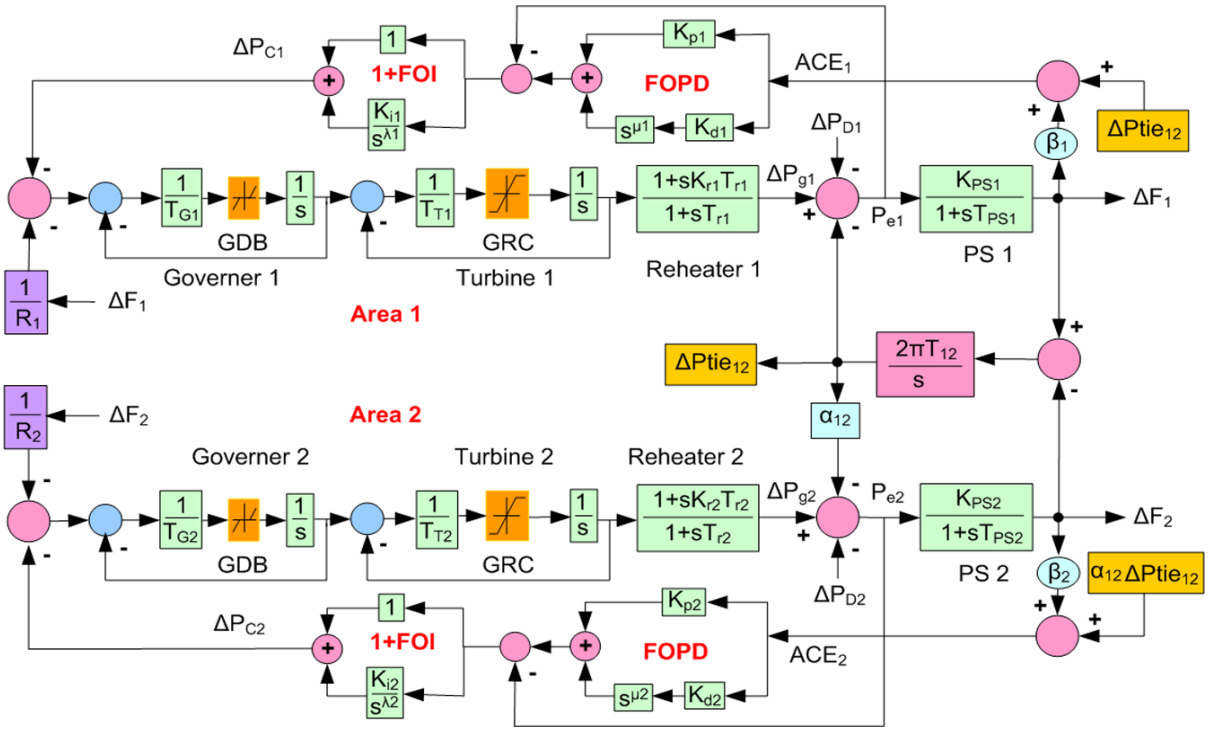

Fig. 1 Two-areas reheat thermal PS with FOPD-(1+FOI) cascade control

The generalized dynamics of multiarea PS in the form of a transfer function (TF) are described as follows [2]:

Governor $TF = G_{G,i}(s) = \frac{1}{(1+sT_{Gi})}$ (1)

Reheated turbine $TF = G_{T,i}(s) = \frac{1}{(1+sT_{Ti})}\frac{(1+sK_{ri}T_{ri})}{(1+sT_{ri})}$ (2)

PS $TF = G_{PS,i}(s) = \frac{K_{PSi}}{(1+sT_{PSi})}$ (3)

where $i = 1, 2 \ldots\ldots N$.

3. Proposed Controller Design

3.1 Fractional order (FO) calculus

The generalized form of integer order calculus is the FO calculus that converts the integer-order differential and integral operators to the FO. ${}_{A}\mathrm{Q}_{t}^{\bar{\alpha}}$ is the fractional operator responsible for the transform. Based on the sign of $\bar{\alpha}$, the differentiation or integration operation is decided. The modeling of the fractional operator is as follows [46]:

$$ {}_{A}\mathrm{Q}_{t}^{\bar{\alpha}} = \begin{cases} \frac{d^{\bar{\alpha}}}{dt^{\bar{\alpha}}}, & \bar{\alpha} > 1 \\ 1, & \bar{\alpha} = 0 \\ \int_{\bar{\alpha}}^{t}(dt)^{\bar{\alpha}}, & \bar{\alpha} < 1 \end{cases} \quad (4)$$

There is various literature available for the definitions of the FO functions. A few definitions are the Grunwald-Letnikov (G-L) definition, Riemann-Liouville (R-L) definition, and the Caputo definition [46].

The most used definition is R-L, which is as follows [46]:

$$ {}_{A}\mathrm{Q}_{t}^{\bar{\alpha}} = \frac{1}{\Gamma(k-\bar{\alpha})}\frac{d^{k}}{dt^{k}}\int_{\bar{\alpha}}^{t}\frac{x(\tau)}{(t-\tau)^{1-(k-\bar{\alpha})}}\,d\tau \quad (5)$$

where, $\Gamma(\cdot)$ is the Euler's gamma function, and k is an integer $k-1 < \bar{\alpha} \leq k$. Before using the FO controller in real or simulation applications, it is required the approximation of FO differentiators and integrators with corresponding integer-order counterparts. Moreover, the FO differentiators and integrators are infinite-dimensional in nature, so before putting them into practice, must be band limited. To band limit them, various approximation schemes are available such as Matsuda approximation, Carlson approximation, Oustaloup's recursive approximation, and Crone approximation [47]. In this proposed work, Oustaloup's recursive approximation is employed to realize FO controllers within the frequency range of ($\omega_l = 0.001$, $\omega_u = 1000$) rad/s. Using this, FO differentiator and integrator are approximated via recursive distribution of zeroes and poles as:

$$ s^{\bar{\alpha}} = M\prod_{k=1}^{K}\frac{1+\left({}^{s}/_{\omega_{z,k}}\right)}{1+\left({}^{s}/_{\omega_{p,k}}\right)} \quad (6)$$

Frequencies of zeros and poles are:

$$ \begin{cases} \omega_{z1} = \omega_l\sqrt{\eta} \\ \omega_{z,k} = \omega_{z,k}\varepsilon, \;\; k = 1,2,3,\ldots\ldots,K \\ \omega_{z,k+1} = \omega_{p,k}\sqrt{\eta}, \;\; k = 1,2,3,\ldots\ldots,K-1 \\ \varepsilon = \left(\frac{\omega_u}{\omega_l}\right)^{{\bar{\alpha}}/{K}} \\ \eta = \left(\frac{\omega_u}{\omega_l}\right)^{{(1-\bar{\alpha})}/{K}} \end{cases} \quad (7)$$

In this work, the authors have utilized the fractional-order modeling and control (FOMCON) toolbox for the designing of the proposed FO controller.

3.2 Cascade controller

The key feature of the cascade controller is to mitigate the impact of disturbance propagation through another part of the system since it gives an extra feedback path, i.e., sensor for restricting and reducing disturbance quickly before the final output [34]. It consists of two loops, as revealed in Fig. 2.

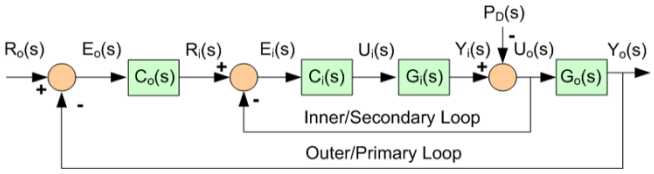

Fig. 2 Structure of proposed cascade controller

The outer loop is considered the primary loop that carries $Y_o(s)$ as the controlled output. Its gain $G_o(s)$ is affected by the power demand $P_D(s)$ and expressed as:

$$ Y_o(s) = G_o(s)U_o(s) = G_o(s)\big(Y_i(s) - P_D(s)\big) \quad (8)$$

where, $U_o(s)$ is the input signal to $G_o(s)$, which is equivalent to the inner loop's processed output $Y_i(s)$. The outer loop's controller is $C_o(s)$, which will supervise $Y_o(s)$ to receive a reference signal $R_o(s)$. The inner loop is considered the secondary loop and will process the inner loop's gain $G_i(s)$ and formulated as:

$$ Y_i(s) = G_i(s)U_i(s) \quad (9)$$

where, $U_i(s)$ is the input signal to the $G_i(s)$ and $C_i(s)$ is the controller for the inner loop. Its objective is to reduce the inner process gain deviations impact. The complete transfer function for the cascade control is revealed as follows:

$$ Y_o(s) = \left[\frac{G_o(s)G_i(s)C_o(s)C_i(s)}{1+G_o(s)C_o(s)+G_o(s)G_i(s)C_o(s)C_i(s)}\right]R_o(s) - \left[\frac{G_o(s)}{1+G_o(s)C_o(s)+G_o(s)G_i(s)C_o(s)C_i(s)}\right]P_D(s) \quad (10)$$

In this work, the proposed cascade controller is FOPD-(1+FOI), where the primary/outer loop controller $C_o(s)$ is FOPD, and the inner loop controller $C_i(s)$ is (1+FOI), as depicted in Fig. 1. The two controllers can be described in the generalized form as:

$$ C_{o,i}(s) = K_{pi} + K_{di}s^{\mu i} \quad (11)$$

$$ C_{i,i}(s) = 1 + \frac{K_{ii}}{s^{\lambda i}} \quad (12)$$

where i=1 for area-1 and i=2 for area-2, and K_{pi} is the proportional gain, K_{di} is differential gain, μi is differential fractional order, K_{ii} is integral gains, and λi is integral fractional order. Due to the cascade connection of two controllers, it obtains the property of disturbance rejection before they outspread to another system. From Fig. 1, the resulting equations for area-1 are as:

$$ \Delta F_1 = G_{PS,1}(s)P_{e1} \quad (13)$$

$$ P_{e1} = \Delta P_{g1} - \Delta Ptie_{12} - \Delta P_{D1} \quad (14)$$

$$ \Delta P_{g1} = G_{G,1}(s)G_{T,1}(s)\left(-\Delta P_{c1} - \frac{1}{R_1}\Delta F_1\right) \quad (15)$$

$$ \Delta P_{c1} = C_{i,1}(s)\big(C_{o,1}(s) * ACE_1 - P_{e1}\big) \quad (16)$$

$$ACE_1 = \beta_1 \Delta F_1 + \Delta Ptie_{12} \quad (17)$$

$$\Delta Ptie_{12} = \frac{2\pi T_{12}}{s}(\Delta F_1 - \Delta F_2) \quad (18)$$

To establish the independent relations for area-1, considering the $\Delta F_2 = 0$ in (18), and from (13)-(18), yield (19). Similarly, the decoupled equation for area-2 is derived and represented by (20). To obtain the optimal controller performance, a total of ten parameters in both areas of PS must be optimized. WHO is chosen for the simultaneous optimization of these parameters. The optimized value of any controller depends on the appropriate objective function (J).

$$\Delta F_1 = -\left[\frac{G_{PS,1}(s)}{1+\frac{2\pi T_{12}}{s}G_{PS,1}(s)-G_{G,1}(s)G_{T,1}(s)C_{i,1}(s)+G_{G,1}(s)G_{T,1}(s)G_{PS,1}(s)C_{i,1}(s)C_{o,1}(s)\left(\beta_1+\frac{2\pi T_{12}}{s}\right)+\frac{G_{G,1}(s)G_{T,1}(s)G_{PS,1}(s)}{R_1}}\right]\Delta P_{D1} \quad (19)$$

$$\Delta F_2 = -\left[\frac{G_{PS,2}(s)}{1+\frac{2\pi T_{12}}{s}G_{PS,2}(s)-G_{G,2}(s)G_{T,2}(s)C_{i,2}(s)+G_{G,2}(s)G_{T,2}(s)G_{PS,2}(s)C_{i,2}(s)C_{o,2}(s)\left(\beta_2+\frac{2\pi T_{12}}{s}\right)+\frac{G_{G,2}(s)G_{T,2}(s)G_{PS,2}(s)}{R_2}}\right]\Delta P_{D2} \quad (20)$$

Different types of J have been utilized in the literature as mentioned below:

$$(\text{ISE}) = \int_0^t \{(\Delta F_1)^2 + (\Delta F_2)^2 + (\Delta Ptie_{12})^2\}dt \quad (21)$$

$$(\text{ITSE}) = \int_0^t t\{(\Delta F_1)^2 + (\Delta F_2)^2 + (\Delta Ptie_{12})^2\}dt \quad (22)$$

$$(\text{IAE}) = \int_0^t \{|\Delta F_1| + |\Delta F_2| + |\Delta Ptie_{12}|\}dt \quad (23)$$

$$(\text{ITAE}) = \int_0^t t\{|\Delta F_1| + |\Delta F_2| + |\Delta Ptie_{12}|\}dt \quad (24)$$

where t is the simulation time, ΔF_1, ΔF_2 and ΔPtie_{12} are the responses against step load perturbation (SLP). Controlled response with damped oscillations and less settling time are obtained while dealing with ITAE objective function, and it is implemented in LFM studies very frequently [6], [33-35] compared to other variants; hence, it is considered in the presented study. The design of the controller is a constrained tuning task, where the bounds parameter of the controller works as a constraint. Hence, lessen J considering to:

$$\begin{Bmatrix} K_{p1}^{min} \le K_{p1} \le K_{p1}^{max} \\ K_{d1}^{min} \le K_{d1} \le K_{d1}^{max} \\ K_{i1}^{min} \le K_{i1} \le K_{i1}^{max} \\ K_{p2}^{min} \le K_{p2} \le K_{p2}^{max} \\ K_{d2}^{min} \le K_{d2} \le K_{d2}^{max} \\ K_{i2}^{min} \le K_{i2} \le K_{i2}^{max} \\ \mu 1^{min} \le \mu 1 \le \mu 1^{max} \\ \mu 2^{min} \le \mu 2 \le \mu 2^{max} \\ \lambda 1^{min} \le \lambda 1 \le \lambda 1^{max} \\ \lambda 2^{min} \le \lambda 2 \le \lambda 2^{max} \end{Bmatrix} \quad (25)$$

These ten parameters are obtained via running WHO to enhance the complete system performance of the proposed interconnected PS.

4. Wild Horse Optimizer (WHO)

The behavior of non-territorial horses is the motivation for this optimization technique which was proposed in 2021 [43]. WHO consists of five key steps; in the first step initial population is created, and horse groups are formed with the selection of leaders; mating and grazing of horses is the second step; in the third step, the groups are leaded by the leader (stallion); the process of exchange and selection of leaders have occurred in the fourth step, and in the final step, the best solution is obtained. For proper communication, stallions are located near the mares, and mating occurs at any time. Generally, foals are started grazing in the initial week and have less rest time as they become older. The random initial population is considered as follows:

$$(\vec{x}) = \{\vec{x}_1, \vec{x}_2, \vec{x}_3 \dots\dots\dots\dots\dots, \vec{x}_n\} \quad (26)$$

The process of evaluation of this random population is performed via the target function. The target function is evaluated as:

$$(\vec{O}) = \{O_1, O_2, O_3 \dots\dots\dots\dots\dots O_n\} \quad (27)$$

Firstly, the population is divided into various groups. The number of groups is $G = [n \times ps]$, where n is the number of members and ps is the percentage of stallions, and it is the control parameter in this algorithm. This population division is revealed in Fig. 3.

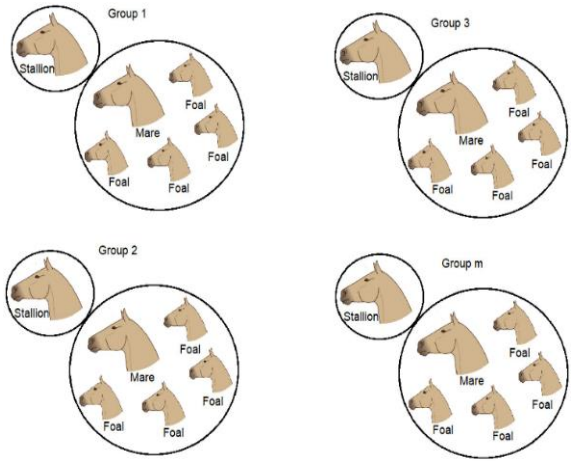

Fig. 3 Formation of horse groups in initial population [43]

To obtain the grazing behavior, the stallion is placed in the center of the grazing area, and other members search around the center. The grazing behavior is simulated as:

$$\bar{X}_{i,G}^{j} = 2Z\cos(2\pi RZ) \times \left(Stallion^{j} - X_{i,G}^{j}\right) + Stallion^{j} \quad (28)$$

where, $\bar{X}_{i,G}^{j}$ is the new position of group member while grazing, the current position of foal or mare is $X_{i,G}^{j}$, the position of the group leader is $Stallion^{j}$, R is uniform distribution in $[-2, 2]$, Z is the adaptive mechanism calculated as:

$$P = \vec{R}_1 < TDR; \quad IDX = (P == 0); \quad Z = R_2 \Theta IDX + \vec{R}_3 \Theta(\sim IDX) \quad (29)$$

P is a vector with values 0 and 1, $\vec{R}_1, R_2$ and $\vec{R}_3$ are random vectors with [0,1], IDX is the index of a random vector $\vec{R}_1$ satisfying $(P == 0)$, TDR is an adaptive parameter with an initial value 1 and decreased to 0 as the execution of the algorithm starts as:

$$TDR = 1 - iter \times \left(\frac{1}{maxiter}\right) \quad (30)$$

where, $iter$ and $maxiter$ are the current and maximum iterations. One of the important behavior of horses is separating foals from the group and mating them while compared with other animals. The mating process of horses is simulated as:

$$X_{G,K}^{p} = Crossover\left(X_{G,i}^{q}, X_{G,i}^{z}\right) \quad i \neq j \neq k, p = q = end,$$
$$Crossover = Mean \tag{31}$$

In group k, the position of horse p is $X_{G,K}^{p}$ and gives it a place who have to leave group i and j. The position of foal q is $X_{G,i}^{q}$ from group i, it mated with a horse (z) with position $\left(X_{G,i}^{z}\right)$, which leaves group j. The group leader has the capability to lead the group to an appropriate area (water hole), and this process is simulated by:

$$\overline{Stallion_{G_i}} = \begin{Bmatrix} 2Z\cos(2\pi RZ) \times \left(WH - Stallion_{G_i}\right) + WH \;\; if R_3 > 0.5 \\ 2Z\cos(2\pi RZ) \times \left(WH - Stallion_{G_i}\right) - WH \;\; if R_3 \leq 0.5 \end{Bmatrix} \tag{32}$$

$$\overline{Stallion_{G_i}} = \begin{Bmatrix} X_{G,i} \quad if\cos t\left(X_{G,i}\right) < \cos t\left(Stallion_{G_i}\right) \\ Stallion_{G_i} \quad if\cos t\left(X_{G,i}\right) > \cos t\left(Stallion_{G_i}\right) \end{Bmatrix} \tag{33}$$

where, the next position of leader is $\overline{Stallion_{G_i}}$ of the group i, the position of water hole is WH, and the current position of leader is $Stallion_{G_i}$ of the group i. The flowchart of the WHO scheme is shown in Fig. 4.

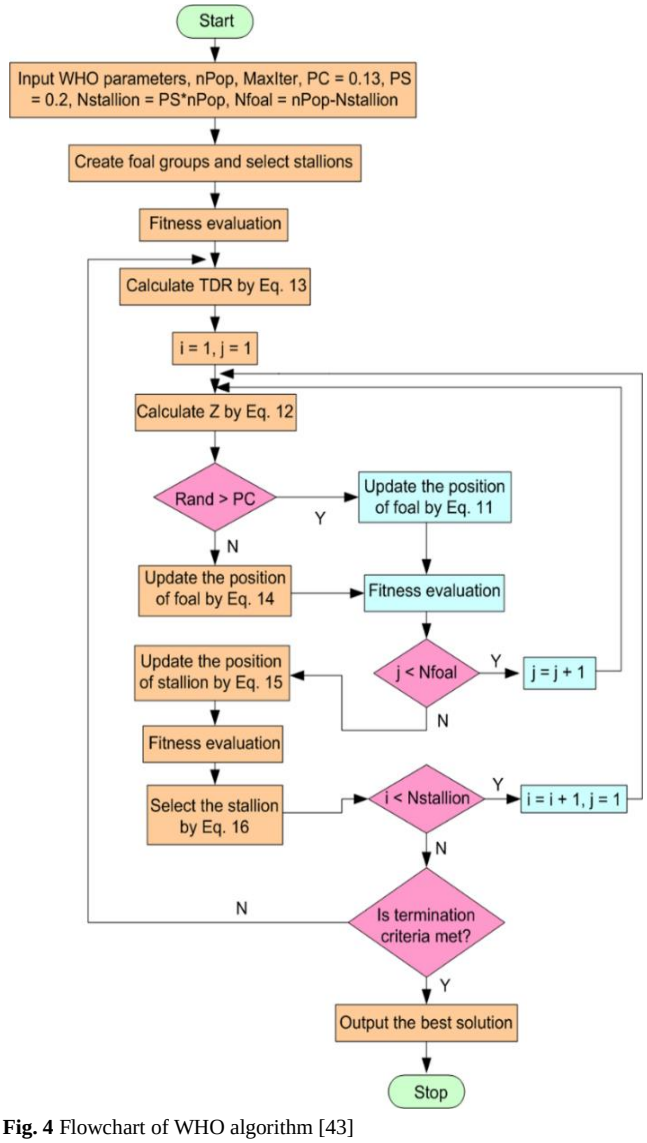

Fig. 4 Flowchart of WHO algorithm [43]

5. Results and Discussion

5.1 Test case-1 with SLP of 10% in area-1

The proposed WHO:FOPD-(1+FOI) fractional cascade controller is implemented on an interconnected reheat thermal PS. A state-of-the-art of five optimization techniques as MBA, GWO, MGWO, BWOA, and WHO, and four different types of controllers as PID, FOPID, PI-PD, FOPD-(1+FOI) for the LFM have been briefed. To benchmark the superior performance of fractional cascade controller, the convergence rates of WHO:PID, WHO:FOPID, WHO:PI-PD, and WHO:FOPD-(1+FOI) are depicted in Figs. 5(a)-(d), respectively, and analyzed in Table 1.

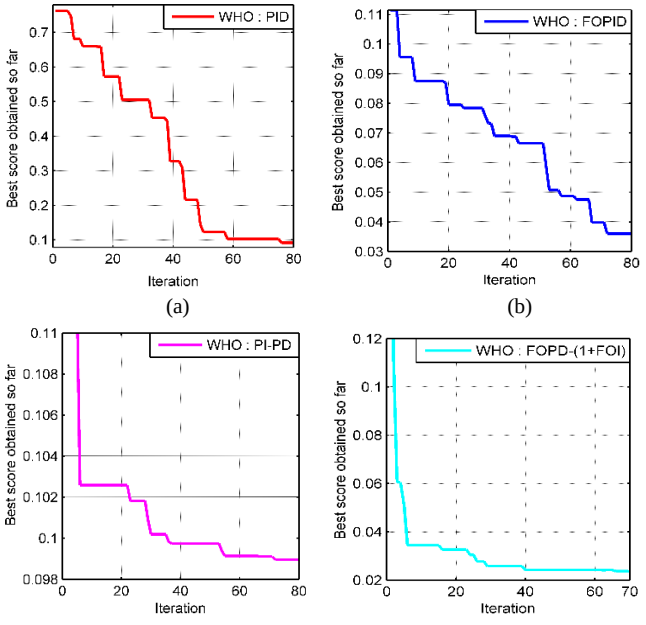

Fig. 5 Convergence of WHO tuned (a) PID, (b) FOPID, (c) PI-PD and (d) FOPD-(1+FOI)

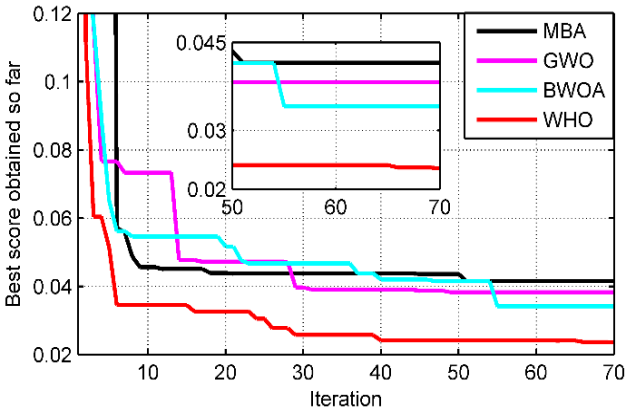

Fig. 6 Convergence rate of various metaheuristics for FOPD-(1+FOI) controller

Table 1: Convergence analysis of all designed control schemes

Techniques	Iterations	Minimum J
WHO:PID	77	0.1
WHO:FOPID	72	0.038
WHO:PI-PD	75	0.099
MBA:FOPD-(1+FOI)	53	0.0415
GWO:FOPD-(1+FOI)	49	0.0395
BWOA:FOPD-(1+FOI)	56	0.0366
Proposed	**40**	**0.0234**

In the case of WHO:PID the best score is obtained after 77 iterations with a minimum J of 0.1; for WHO:FOPID the best score is obtained after 72 iterations with a minimum J of 0.038; for WHO:PI-PD the best score is obtained after 75 iterations with a minimum J of 0.099, while for the proposed WHO:FOPD-(1+FOI) controller the best score is obtained after 40 iterations with minimum J of 0.0234. So, from the above-mentioned analysis and results revealed in Figs 5(a)-(d) it is concluded that the proposed fractional cascade controller is fast enough and cost-effective in comparison to full order controller, fractional-order controller, and full order cascade controller. Fig. 6 and Table 1 have revealed the convergence of different meta-heuristics applied to FOPD-(1+FOI) controller. It is noted that the best score with faster convergence and cost-effectiveness is obtained in the case of the proposed WHO scheme with a minimum J of 0.0234 in comparison to MBA, GWO, and BWOA. An SLP of 10% is provided in area-1, and the responses as ΔF_1, ΔF_2 and $\Delta Ptie$ via the implementation of various control schemes are presented in Figs 7(a)-(c), respectively.

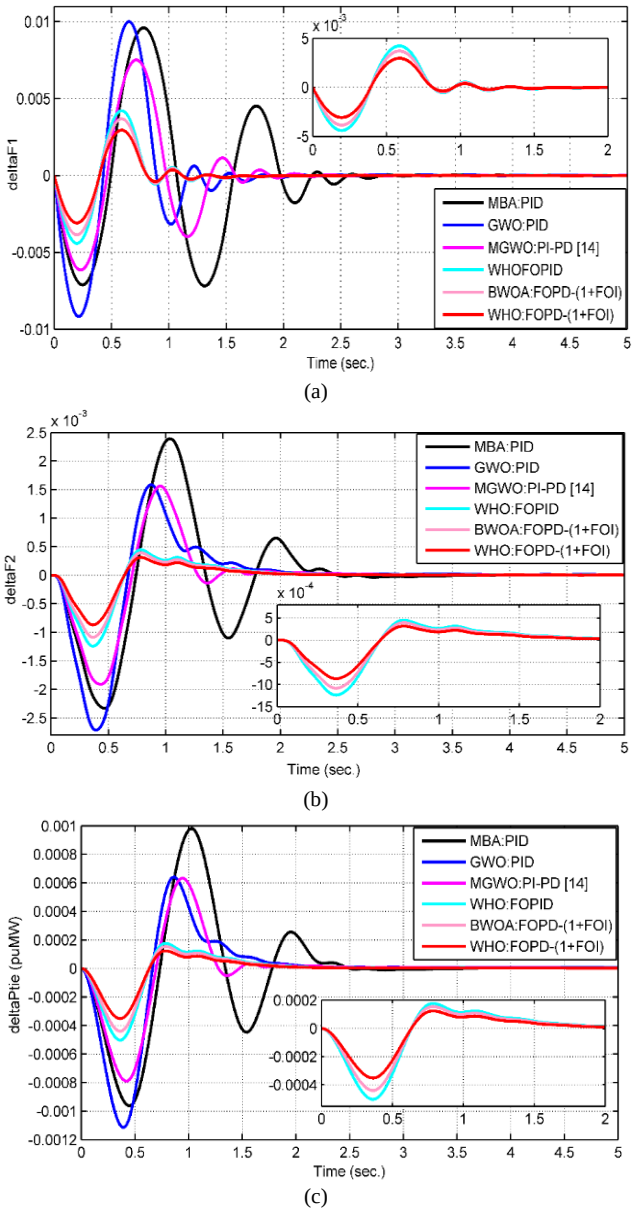

Fig. 7 Performance of controllers with SLP of 10% in area 1 (a) ΔF_1 (Hz) (b) ΔF_2 (Hz), and (c) $\Delta Ptie$

The maximum OS in ΔF_1 is 0.01 Hz (GWO:PID) and minimum for the proposed WHO:FOPD-(1+FOI) controller (0.0023 Hz). The maximum OS of 2.4×10^{-3} Hz is obtained for ΔF_2 in the case of MBA:PID and minimum are noted for the proposed controller as 0.24×10^{-3}. While analyzing the US, the maximum US in ΔF_1 is 0.0097 Hz (GWO:PID), and the minimum US is 0.0029 Hz obtained for the proposed control scheme. As depicted in Fig. 7(b) and Table 2, the USs in ΔF_2 are 0.0023 Hz, 0.0028 Hz, 0.00192 Hz, 0.00125 Hz, 0.0011 Hz, and 0.0008 Hz for MBA:PID, GWO:PID, MGWO:PI-PD, WHO: FOPID, BWOA:FOPD-(1+FOI) and proposed controller respectively. Moreover, the minimum US of the order of 0.00035 is obtained for WHO:FOPD-(1+FOI) controller while dealing with the response of $\Delta Ptie$. While analyzing the settling time (t_s) of ΔF_1, the t_s of 3.3 sec., 2.3 sec., 2.4 sec., 1.5 sec., 1.3 sec., and 1.3 sec. for MBA:PID, GWO:PID, MGWO:PI-PD, WHO: FOPID, BWOA: FOPD-(1+FOI) and proposed controller respectively is obtained. The maximum t_s are 3.55 sec., and 3 sec. for ΔF_2 and $\Delta Ptie$ respectively for MBA:PID controller, and the minimum is noted for the proposed WHO:FOPD-(1+FOI) controller as mentioned in Table 2. Further while dealing with the error constants for ΔF_1, ΔF_2 and $\Delta Ptie$, the minimum of IAE, ITAE, ISE, and ITSE is noted for the proposed controller, and the maximum is noted for MBA:PID controller.

5.2 Test case-2 with SLP of 20% in area-1 and SLP of 10% in area-2

In this section, the analysis of the performance of all applied controllers for LFM is evaluated. Figs. 8(a)-(c) show the response of ΔF_1, ΔF_2 and $\Delta Ptie$ and vivid comparative analysis of the controller performance is given in Table 3.

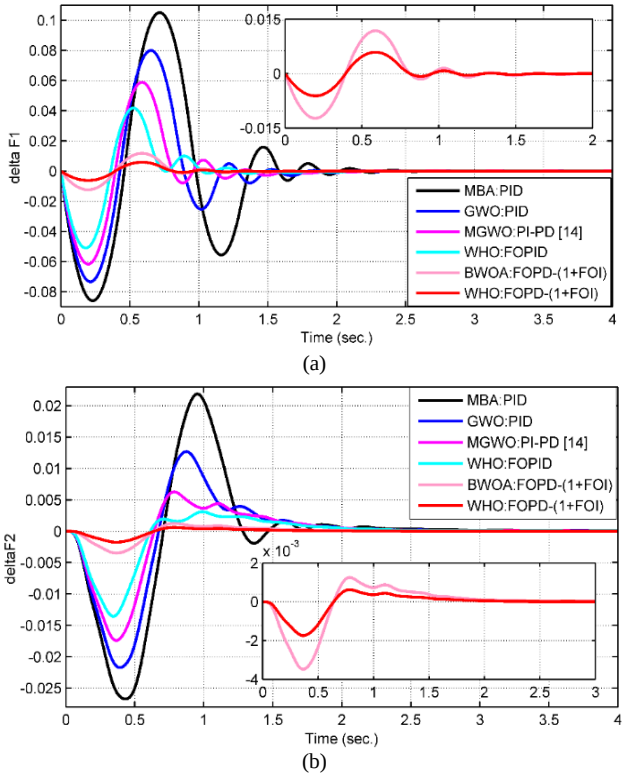

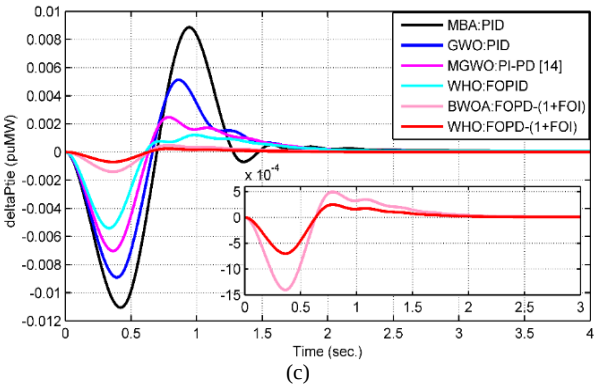

(c)

Fig. 8 Performance of controllers with SLP of 20% in Area-1 and SLP of 10% (a) ΔF_1 (Hz), (b) ΔF_2 (Hz), and (c) $\Delta Ptie$

The maximum OS (0.11 Hz) of ΔF_1 is obtained in the case of MBA-PID, and the minimum OS (0.0065 Hz) is for the proposed controller. For ΔF_2 OSs are 0.024 Hz, 0.013 Hz, 0.0065 Hz, 0.017 Hz, 0.0013 Hz, and 0.0008 Hz for MBA:PID, GWO:PID, MGWO:PI-PD, WHO:FOPID, BWOA:FOPD-(1+FOI) and proposed controller respectively, while the USs are 0.028 Hz, 0.022 Hz, 0.018 Hz, 0.014 Hz, 0.0036 Hz, and 0.0018 Hz respectively for the same applied controller. While dealing with the $\Delta Ptie$, the maximum OS and US are 0.009 and 0.011 for MBA:PID, and the minimum OS and US are 0.0002 and 0.0006 for the proposed controller. From Figs. 8(a)-(c) and Table 3, the t_s (ΔF_1) are 2.4 sec., 2 sec., 1.9 sec., 1.8 sec., 1.3 sec., and 1.2 sec., the t_s (ΔF_2) are 2.6 sec., 2.5 sec., 2.3 sec., 2.4 sec., 2.2 sec., 2 sec. for MBA:PID, GWO:PID, MGWO:PI-PD, WHO:FOPID, BWOA:FOPD-(1+FOI), and proposed controller respectively. In the case of tie-line flow the t_s are, 3.2 sec., 2.7 sec., 2.4 sec., 2.2 sec., 2 sec., 2 sec. for MBA:PID, GWO:PID, MGWO:PI-PD, WHO:FOPID, BWOA:FOPD-(1+FOI) and WHO:FOPD-(1+FOI) controllers respectively. While dealing with the error constants, the minimum of IAE, ITAE, ISE, and ITSE is obtained for the proposed controller, and the maximum IAE, ITAE, ISE, and ITSE is obtained for MBA:PID controller for ΔF_1, ΔF_2 and $\Delta Ptie$ as tabulated in Table 3.

Table 2: Comparative analysis of different control schemes for SLP of 10% in area-1

SLP of 10% in area-1							
Performance Indices		**MBA: PID**	**GWO: PID**	**MGWO: PI-PD [14]**	**WHO: FOPID**	**BWOA: FOPD-(1+FOI)**	**WHO: FOPD-(1+FOI)**
Overshoot (OS)	ΔF_1(Hz)	0.00950	0.0100	0.0078	0.00410	0.0038	**0.0023**
	ΔF_2(Hz)	0.00240	0.00152	0.00151	0.00048	0.00046	**0.00024**
	$\Delta Ptie$(puMW)	0.00100	0.00062	0.00062	0.00019	0.00017	**0.0001**
Undershoot (US)	ΔF_1(Hz)	0.00770	0.0097	0.00610	0.0043	0.0039	**0.0029**
	ΔF_2(Hz)	0.00230	0.0028	0.00192	0.00125	0.0011	**0.00080**
	$\Delta Ptie$(puMW)	0.00095	0.0011	0.0008	0.0005	0.00045	**0.00035**
Rise time (t_r) (sec.)	ΔF_1	0.50000	0.4500	0.4700	0.4000	0.4000	**0.4000**
	ΔF_2	0.80000	0.7000	0.7500	0.6500	0.6500	**0.6500**
	$\Delta Ptie$	0.75000	0.7100	0.7300	0.6200	0.6200	**0.6200**
Settling time (t_s) (sec.)	ΔF_1	3.3000	2.3000	2.4000	1.5000	1.3000	**1.3000**
	ΔF_2	3.5500	2.4000	2.3000	2.0000	1.9000	**1.9000**
	$\Delta Ptie$	3.000	3.0000	2.4000	1.9000	1.9000	**1.9000**
ΔF_1	IAE	6.1×10^{-1}	7.8×10^{-2}	4.3×10^{-2}	4.0×10^{-2}	3.9×10^{-2}	$\mathbf{3.3\times 10^{-2}}$
	$ITAE$	5.8×10^{-1}	6.5×10^{-2}	3.9×10^{-2}	3.6×10^{-2}	3.32×10^{-2}	$\mathbf{2.9\times 10^{-2}}$
	ISE	7.6×10^{-2}	8.85×10^{-3}	2.2×10^{-3}	1.9×10^{-3}	1.7×10^{-3}	$\mathbf{1.1\times 10^{-3}}$
	$ITSE$	8.1×10^{-3}	9.3×10^{-4}	4.1×10^{-4}	3.7×10^{-4}	3.4×10^{-4}	$\mathbf{3.1\times 10^{-4}}$
ΔF_2	IAE	5.65×10^{-1}	7.1×10^{-2}	3.9×10^{-2}	3.8×10^{-2}	3.6×10^{-2}	$\mathbf{2.95\times 10^{-2}}$
	$ITAE$	5.23×10^{-1}	5.8×10^{-2}	3.74×10^{-2}	3.3×10^{-2}	3.12×10^{-2}	$\mathbf{2.65\times 10^{-2}}$
	ISE	6.23×10^{-2}	6.25×10^{-3}	1.9×10^{-3}	1.6×10^{-3}	1.3×10^{-3}	$\mathbf{8.21\times 10^{-4}}$
	$ITSE$	7.43×10^{-3}	7.54×10^{-4}	3.8×10^{-4}	3.3×10^{-4}	2.3×10^{-4}	$\mathbf{2.3\times 10^{-4}}$
$\Delta Ptie$	IAE	5.28×10^{-1}	6.85×10^{-2}	3.25×10^{-2}	2.65×10^{-2}	3.55×10^{-2}	$\mathbf{2.85\times 10^{-2}}$
	$ITAE$	4.91×10^{-1}	5.61×10^{-2}	3.54×10^{-2}	2.81×10^{-2}	2.91×10^{-2}	$\mathbf{2.54\times 10^{-2}}$
	ISE	5.96×10^{-2}	5.89×10^{-3}	1.81×10^{-3}	1.35×10^{-3}	1.25×10^{-3}	$\mathbf{7.86\times 10^{-4}}$
	$ITSE$	7.13×10^{-3}	7.21×10^{-4}	3.6×10^{-4}	2.86×10^{-4}	2.12×10^{-4}	$\mathbf{2.23\times 10^{-4}}$

Table 3: Comparative analysis of different control schemes for SLP of 20% in area-1 and SLP of 10% in area-2

SLP of 20% in area-1 and SLP of 10% in area-2							
Performance Indices		**MBA: PID**	**GWO: PID**	**MGWO: PI-PD [14]**	**WHO: FOPID**	**BWOA: FOPD-(1+FOI)**	**WHO: FOPD-(1+FOI)**
OS	ΔF_1(Hz)	0.110	0.0800	0.0600	0.0420	0.0130	**0.0065**
	ΔF_2(Hz)	0.024	0.0130	0.0065	0.0170	0.0013	**0.0008**
	$\Delta Ptie$(puMW)	0.009	0.0055	0.0028	0.0015	0.0005	**0.0002**
US	ΔF_1(Hz)	0.090	0.0750	0.0610	0.0500	0.0130	**0.0065**
	ΔF_2(Hz)	0.028	0.0220	0.0180	0.0140	0.0036	**0.0018**
	$\Delta Ptie$(puMW)	0.011	0.0090	0.0070	0.0057	0.0014	**0.0006**
t_r (sec.)	ΔF_1	0.480	0.4600	0.4200	0.3800	0.4200	**0.4200**

	ΔF_2	0.700	0.7200	0.7000	0.6500	0.7000	**0.7000**
	$\Delta Ptie$	0.700	0.6800	0.6600	0.5800	0.6600	**0.6600**
t_s **(sec.)**	ΔF_1	2.400	2.0000	1.9000	1.8000	1.3000	**1.2000**
	ΔF_2	2.600	2.5000	2.3000	2.4000	2.2000	**2.0000**
	$\Delta Ptie$	3.200	2.7000	2.4000	2.2000	2.0000	**2.0000**
ΔF_1	IAE	6.1×10^{-1}	7.8×10^{-2}	4.3×10^{-2}	4.0×10^{-2}	3.9×10^{-2}	$\mathbf{3.3\times 10^{-2}}$
	$ITAE$	5.8×10^{-1}	6.5×10^{-2}	3.9×10^{-2}	3.6×10^{-2}	3.32×10^{-2}	$\mathbf{2.9\times 10^{-2}}$
	ISE	7.6×10^{-2}	8.85×10^{-3}	2.2×10^{-3}	1.9×10^{-3}	1.7×10^{-3}	$\mathbf{1.1\times 10^{-3}}$
	$ITSE$	8.1×10^{-3}	9.3×10^{-4}	4.1×10^{-4}	3.7×10^{-4}	3.4×10^{-4}	$\mathbf{3.1\times 10^{-4}}$
ΔF_2	IAE	5.65×10^{-1}	7.1×10^{-2}	3.9×10^{-2}	3.8×10^{-2}	3.6×10^{-2}	$\mathbf{2.95\times 10^{-2}}$
	$ITAE$	5.23×10^{-1}	5.8×10^{-2}	3.74×10^{-2}	3.3×10^{-2}	3.12×10^{-2}	$\mathbf{2.65\times 10^{-2}}$
	ISE	6.23×10^{-2}	6.25×10^{-3}	1.9×10^{-3}	1.6×10^{-3}	1.3×10^{-3}	$\mathbf{8.21\times 10^{-4}}$
	$ITSE$	7.43×10^{-3}	7.54×10^{-4}	3.8×10^{-4}	3.3×10^{-4}	2.3×10^{-4}	$\mathbf{2.3\times 10^{-4}}$
$\Delta Ptie$	IAE	5.28×10^{-1}	6.85×10^{-2}	3.25×10^{-2}	2.65×10^{-2}	3.55×10^{-2}	$\mathbf{2.85\times 10^{-2}}$
	$ITAE$	4.91×10^{-1}	5.61×10^{-2}	3.54×10^{-2}	2.81×10^{-2}	2.91×10^{-2}	$\mathbf{2.54\times 10^{-2}}$
	ISE	5.96×10^{-2}	5.89×10^{-3}	1.81×10^{-3}	1.35×10^{-3}	1.25×10^{-3}	$\mathbf{7.86\times 10^{-4}}$
	$ITSE$	7.13×10^{-3}	7.21×10^{-4}	3.6×10^{-4}	2.86×10^{-4}	2.12×10^{-4}	$\mathbf{2.23\times 10^{-4}}$

5.3 Robustness Analysis

In this section, the robustness analysis of the proposed WHO:FOPD-(1+FOI) controller under parametric uncertainties is evaluated. In the practical system, parametric uncertainties may occur in the governor, turbine, reheater, frequency biasing, and governor regulation for both area-1 and area-2 also there will be communication delay in the physical response of all connected elements. The above-mentioned uncertainties will greatly affect the performance of PS; hence a huge number of uncertainties are considered only in the parameters of PS of area-1 (T_{PS1} and K_{PS1}) with SLP of 13% in area-1 and the responses of the proposed controller are depicted in Figs. 9(a)-(c), and 10(a)-(c) with vivid analysis tabulated in Table 4. Firstly, the uncertainties in T_{PS1} as $T_{PS1}/4$ and $4 \times T_{PS1}$ are considered and responses of ΔF_1, ΔF_2 and $\Delta Ptie$ with respect to nominal values are depicted in Figs. 9 (a)-(c) respectively.

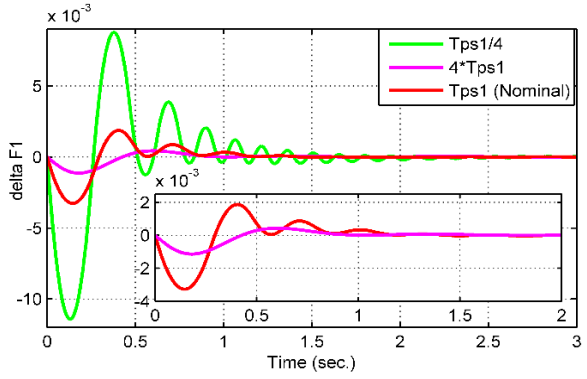

(a)

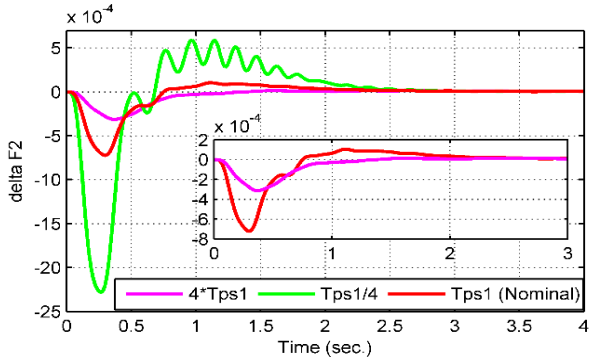

(b)

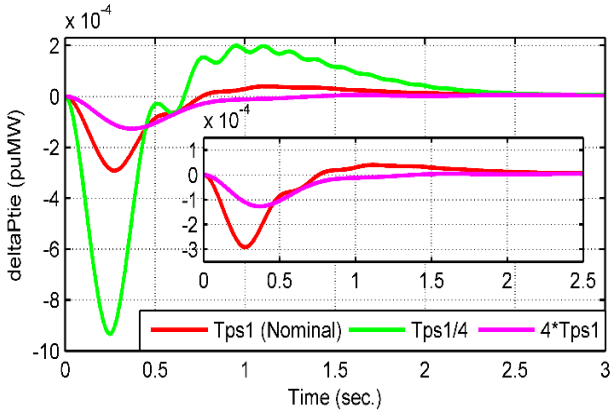

(c)

Fig. 9 Robustness analysis of proposed controller with SLP of 13% in area-1 (a) ΔF_1 (Hz) (b) ΔF_2 (Hz), and (c) $\Delta Ptie$

The maximum OS (0.0097) and US (0.0135) are obtained in ΔF_1 while considering $T_{PS1}/4$. The values of t_s are 2.6 sec., 2.5 sec., and 2.3 sec. are noted for ΔF_1, ΔF_2 and $\Delta Ptie$ respectively for $T_{PS1}/4$. The impact of $4 \times T_{PS1}$ is almost negligible on the performance of the controller as analyzed in Table 4. Moreover, the other uncertainties in K_{PS1} as $3 \times K_{PS1}$ and $K_{PS1}/3$ are considered, and the controller performance is revealed in Figs. 10(a)-(c) and Table 4. The maximum OS (0.0083) and US (0.0092) are obtained in ΔF_1 while considering $3 \times K_{PS1}$ with t_s values are 2.1 sec., 3.1 sec., and 2.3 sec. in ΔF_1, ΔF_2 and $\Delta Ptie$, respectively. The overall effect of $K_{PS1}/3$ is almost negligible as noted in Table 4.

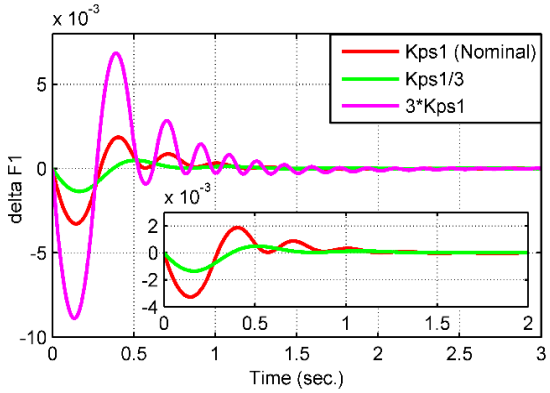

(a)

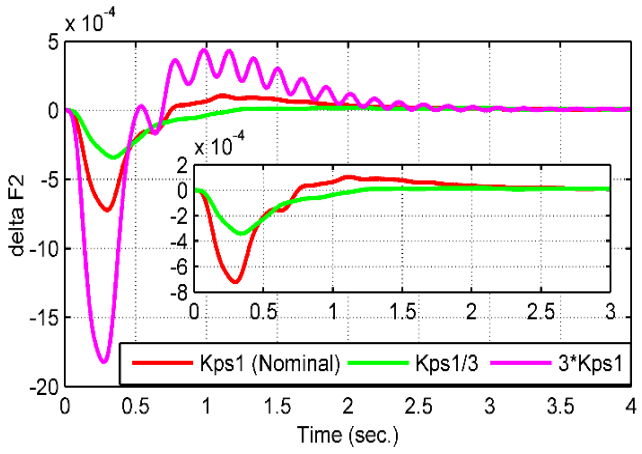

(b)

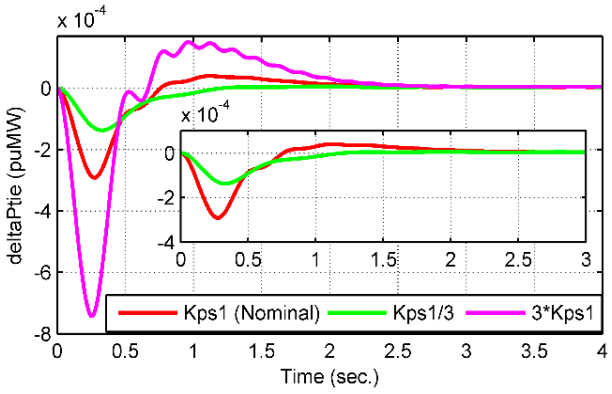

(c)

Fig. 10 Robustness analysis of proposed controller with SLP of 13% in area-1 (a) ΔF_1 (Hz) (b) ΔF_2 (Hz) (c) $\Delta Ptie$

Table 4: Robustness analysis of proposed controller

Proposed controller performance under parametric uncertainties with SLP of 13% in area-1												
Parameters	OS			US			t_r (sec.)			t_s (sec.)		
	ΔF_1(Hz)	ΔF_2(Hz)	$\Delta Ptie$(puMW)	ΔF_1(Hz)	ΔF_2(Hz)	$\Delta Ptie$(puMW)	ΔF_1	ΔF_2	$\Delta Ptie$	ΔF_1	ΔF_2	$\Delta Ptie$
Nominal K_{PS1}, T_{PS1}	0.002	0.00011	Negligible	0.0031	0.00072	0.0003	0.27	0.75	1	1.5	1.9	1
4*T_{PS1}	Negligible	Negligible	Negligible	0.00017	0.00032	0.00012	0.81	1.2	0.91	1	1.2	0.91
T_{PS1}/4	0.0097	0.00064	0.0002	0.0135	0.0023	0.00098	0.25	0.5	0.68	2.6	2.5	2.3
3*K_{PS1}	0.0083	0.00049	0.0002	0.0092	0.0018	0.00093	0.28	0.5	0.62	2.1	3.1	2.3
K_{PS1}/3	Negligible	Negligible	Negligible	0.0018	0.00039	0.00018	0.75	1.3	1.2	0.75	1.3	1.2

5.4 Stability Analysis via Eigenvalue Approach

In order to enhance the dynamic performance of an AGC system, it is necessary to have enough degree of stability. For the purpose of stability evaluation, various methods are available, and eigenvalue is one of them. Before evaluating the eigenvalues, fractional-order terms are converted into their corresponding full-order terms via the SBL method. To show the stability of the proposed controller, the eigenvalues of interconnected two-area PS with WHO-tuned FOPD-(1+FOI) controller are calculated and tabulated in Table 5.

Table 5: Eigenvalues for area-1 and area-2

Area-1	Area-2
$\mathbf{0.0000 + 0.0000i}$	$0.0000 + 0.0000i$
$\mathbf{-4.5032 + 47.1896i}$	$-5.1691 + 43.2310i$
$\mathbf{-4.5032 - 47.1896i}$	$-5.1691 - 43.2310i$
$\mathbf{-12.5000 + 0.0000i}$	$-12.5000 + 0.0000i$
$\mathbf{-12.5000 + 0.0000i}$	$-12.5000 - 0.0000i$
$\mathbf{-3.6374 + 0.0000i}$	$-3.7823 + 0.0000i$
$\mathbf{-3.3333 + 0.0000i}$	$-3.3333 + 0.0000i$
$\mathbf{-3.3333 - 0.0000i}$	$-3.3333 - 0.0000i$
$\mathbf{-2.1923 + 0.0000i}$	$-2.4087 + 0.0000i$
$\mathbf{-1.2608 + 0.0000i}$	$-2.0635 + 0.0000i$
$\mathbf{-1.1381 + 0.0000i}$	$-1.2734 + 0.0000i$
$\mathbf{-0.8615 + 0.0000i}$	$-0.3375 + 0.0000i$
$\mathbf{-0.2001 + 0.0000i}$	$-0.3005 + 0.0000i$
$\mathbf{-0.1836 + 0.0000i}$	$-0.1989 + 0.0000i$
$\mathbf{-0.1531 + 0.0000i}$	$-0.1000 + 0.0000i$
$\mathbf{-0.1000 + 0.0000i}$	$-0.1000 - 0.0000i$
$\mathbf{-0.1000 - 0.0000i}$	$-0.0558 + 0.0000i$
$\mathbf{-0.0500 + 0.0000i}$	$-0.0501 + 0.0000i$
$\mathbf{-0.0500 + 0.0000i}$	$-0.0500 + 0.0000i$
$\mathbf{-0.0500 - 0.0000i}$	$-0.0500 - 0.0000i$
$\mathbf{-0.0285 + 0.0000i}$	$-0.0487 + 0.0000i$
$\mathbf{-0.0228 + 0.0000i}$	$-0.0072 + 0.0000i$
$\mathbf{-0.0007 + 0.0000i}$	$-0.0060 + 0.0000i$

The TF of outer and inner loop controllers for area-1 and area-2 are revealed by Equations (34)-(37).

$$C_{o,1}(s) = 85.675 + 39.829s^{0.994} \cong 85.675 + 39.829s \quad (34)$$

$$C_{i,1}(s) = 1 + \frac{3.1786}{s^{0.912}} \cong 1 + \frac{3.1786}{s^{0.9}} \quad (35)$$

$$C_{o,2}(s) = 52.909 + 14.845s^{0.987} \cong 52.909 + 14.845s \quad (36)$$

$$C_{i,2}(s) = 1 + \frac{1.88296}{s^{0.1374}} \cong 1 + \frac{1.88296}{s^{0.1}} \quad (37)$$

where $s^{0.9} = \frac{242800s^4+328000s^3+60120s^2+1488s+1}{6648s^4+277300s^3+300600s^2+45610s+887.3}$ and $s^{0.1} = \frac{5532s^4+13380s^3+4147s^2+191.5s+1}{4392s^4+13530s^3+5063s^2+284.5s+1.894}$.

It is clearly noted from Table 5 that all the poles of area-1 and area-2 are present in the left half of s-plane. Hence it is concluded that the proposed WHO:FOPD-(1+FOI) cascade controller is able to stabilize the studied interconnected PS system.

5.5 Real Power System Validation

To benchmark the effectiveness of the proposed WHO: FOPD-(1+FOI) controller, a real New England IEEE-39 test bus system is considered, as shown in Fig. 11. Ten reheat-type thermal generating units are present in the standard IEEE-39 bus system and segregated into three areas [3], [45]. For the validation purpose, only two areas, i.e., area-1 and area-2 are considered. The parameters of the IEEE-39 test bus system are presented in Table 6. The generating units of the same area can be replaced by its equivalent single generation unit with equivalent inertia constant (H_e) and speed regulation (R_e) as follows [3, 5]:

$$H_e = \frac{H_1S_1+H_2S_2+\cdots+H_nS_n}{S_{sys}} \quad (38)$$

$$R_e = \frac{1}{\frac{1}{R_1}\left(\frac{S_1}{S_{sys}}\right)+\frac{1}{R_2}\left(\frac{S_2}{S_{sys}}\right)+\cdots\frac{1}{Rn}\left(\frac{S_n}{S_{sys}}\right)} \text{Hz/MW}_{\text{pu}} \quad (39)$$

and $S_{sys} = S_1 + S_2 + \cdots + S_n$ (40)

where, H_i, R_i and S_i are the individual, inertia constant, speed regulation, and machine rating of the i^{th} generating element and G_{U1} to G_{U10} are the generator unit 1 to 10 in all three areas.

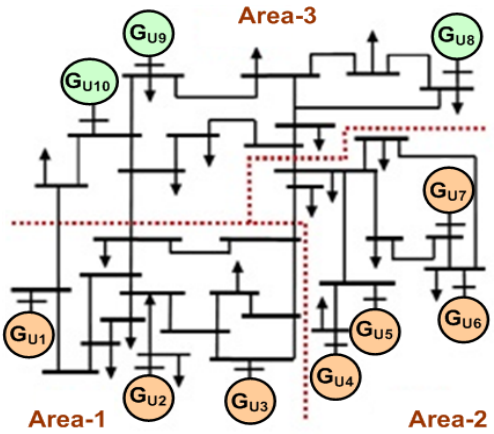

Fig. 11 New England IEEE-39 bus [3], [45]

Table 6: IEEE-39 test bus system parameters [3,5]

Area No.	Unit No.	H	R_d (Hz/MW$_{pu}$)	D (MW$_{pu}$/Hz)	T_g (s)	T_t (s)
1	G_{U1}	4.0	3.0	8.33×10^{-3}	0.08	0.3
	G_{U2}	3.5	3.0	8.33×10^{-3}	0.08	0.3
	G_{U3}	2.5	1.8	8.33×10^{-3}	0.08	0.3
2	G_{U4}	2.5	2.4	8.33×10^{-3}	0.08	0.3
	G_{U5}	3.0	1.8	8.33×10^{-3}	0.08	0.3
	G_{U6}	4.0	2.1	8.33×10^{-3}	0.08	0.3
	G_{U7}	3.0	1.8	8.33×10^{-3}	0.08	0.3
$\alpha_{12} = -1, \beta_1 = \beta_2 = 0.425 Hz/MW_{p.u.}, 2\pi T_{12} = 0.545$puMW/Hz						

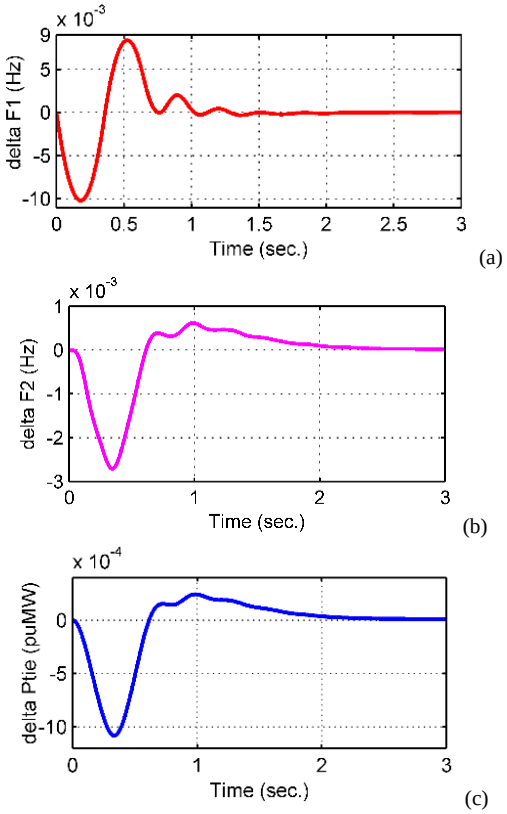

Fig. 12 Controller response for IEEE-39 bus system (a) ΔF_1 (Hz), (b) ΔF_2 (Hz), and (c) $\Delta Ptie$

The proposed controller performance with SLP of 10% in area-1 is shown in Fig. 12. The maximum OS and US in area-1 are 0.0089 Hz and 0.010 Hz, with t_s of 1.3 sec., while dealing with area-2 and tie-line flow, the maximum USs are 0.0029 Hz and 0.0011 puMW with values of t_s are 2.1 sec. and 2 sec. respectively. A vivid comparative analysis of the proposed FOPD-(1+FOI) controller on the simulated and real-time platform is revealed in Table 7.

Table 7: Comparative analysis of proposed controller

SLP of 10% in area-1			
Indices		Simulated	Real-time
OS	ΔF_1(Hz)	0.00230	0.00880
	ΔF_2(Hz)	0.00024	0.00004
	$\Delta Ptie$(puMW)	0.00010	0.00014
US	ΔF_1(Hz)	0.00290	0.01000
	ΔF_2(Hz)	0.00080	0.00270
	$\Delta Ptie$(puMW)	0.00035	0.00110
Rise time (t_r) (sec.)	ΔF_1	0.4000	0.4100
	ΔF_2	0.6500	0.6700
	$\Delta Ptie$	0.6200	0.6700
Settling time (t_s) (sec.)	ΔF_1	1.3000	1.4500
	ΔF_2	1.9000	1.9200
	$\Delta Ptie$	1.9000	1.9200
ΔF_1	IAE	3.3×10^{-2}	4.6×10^{-2}
	$ITAE$	2.9×10^{-2}	4.1×10^{-2}
	ISE	1.1×10^{-3}	2.5×10^{-3}
	$ITSE$	3.1×10^{-4}	4.8×10^{-4}
ΔF_2	IAE	2.95×10^{-2}	4.45×10^{-2}
	$ITAE$	2.65×10^{-2}	4.31×10^{-2}
	ISE	8.21×10^{-4}	8.96×10^{-4}
	$ITSE$	2.3×10^{-4}	2.92×10^{-4}
$\Delta Ptie$	IAE	2.85×10^{-2}	3.48×10^{-2}
	$ITAE$	2.54×10^{-2}	2.94×10^{-2}
	ISE	7.86×10^{-4}	8.93×10^{-4}
	$ITSE$	2.23×10^{-4}	2.65×10^{-4}

6. Conclusion

In this work first time, a novel configuration of WHO-assisted FOPD-(1+FOI) fractional cascade controller is implemented for the load frequency management of an interconnected reheat-type thermal power system network. In the modeling, various non-linearities such as GDB and GRC are considered to replicate the practical scenarios. This controller has the property of both a fractional-order type controller as well as a cascade-type controller. The performance of the proposed controller has been analyzed over five state-of-the-art metaheuristics as MBA, GWO, MGWO, BWOA, and WHO, with four different types of controllers such as PID, PI-PD, FOPID, and FOPD-(1+FOI) under-considered step load perturbations. The obtained results reveal the superiority of the proposed controller in terms of obtained best score (minimization of the objective function), computational cost, speed of convergence, transient response, steady-state response, and considered error rates. While considering the robustness evaluation under practical scenarios of the proposed controller, the performance of the controller is quite satisfactory with lesser

OS and US, and faster settling time. The stability analysis of the proposed scheme is successfully evaluated via the eigenvalue approach. Finally, to benchmark, the performance of the proposed controller on a real power system, an IEEE-39 New England bus system is implemented successfully, and the comparative tabular analysis of simulated and real power system analysis shows satisfactory performance. The future scope of this work will predominately focus on the controller design for interconnected power systems under high renewable penetrations.

7. References

[1] M. Ramesh, A. K. Yadav, and P. K. Pathak, "An extensive review on load frequency control of solar-wind based hybrid renewable energy systems," *Energy Sources, Part A: Recovery, Utilization, and Environmental Effects*, pp. 1-25, 2021.

[2] M. Kumar and Y. V. Hote, "Robust PIDD2 controller design for perturbed load frequency control of an interconnected time-delayed power systems," *IEEE Transactions on Control Systems Technology*, vol. 29, no. 6, pp. 2662-2669, 2021.

[3] N. Pathak and Z. Hu, "Hybrid-peak-area-based performance index criteria for AGC of multi-area power systems," *IEEE Transactions on Industrial Informatics*, vol. 15, no. 11, pp. 5792-5802, 2019.

[4] N. Pathak, T. Bhatti, A. Verma, and I. Nasiruddin, "AGC of two area power system based on different power output control strategies of thermal power generation," *IEEE Transactions on Power Systems*, vol. 33, no. 2, pp. 2040-2052, 2017.

[5] M. Ramesh, A. K. Yadav, and P. K. Pathak, "Intelligent adaptive LFC via power flow management of integrated standalone micro-grid system," *ISA transactions*, vol. 112, pp. 234-250, 2021.

[6] Y. Arya, "ICA assisted FTIλDN controller for AGC performance enrichment of interconnected reheat thermal power systems," *Journal of Ambient Intelligence and Humanized Computing*, pp. 1-17, 2021.

[7] M. H. Cintuglu and O. A. Mohammed, "Behavior modeling and auction architecture of networked microgrids for frequency support," *IEEE Transactions on Industrial Informatics*, vol. 13, no. 4, pp. 1772-1782, 2016.

[8] Y. Arya and N. Kumar, "BFOA-scaled fractional order fuzzy PID controller applied to AGC of multi-area multi-source electric power generating systems," *Swarm and Evolutionary Computation*, vol. 32, pp. 202-218, 2017.

[9] R. Patel, C. Li, L. Meegahapola, B. McGrath, and X. Yu, "Enhancing optimal automatic generation control in a multi-area power system with diverse energy resources," *IEEE Transactions on Power Systems*, vol. 34, no. 5, pp. 3465-3475, 2019.

[10] S. Panda, B. Mohanty, and P. K. Hota, "Hybrid BFOA–PSO algorithm for automatic generation control of linear and nonlinear interconnected power systems," *Applied soft computing*, vol. 13, no. 12, pp. 4718-4730, 2013.

[11] E. S. Ali and S. M. Abd-Elazim, "Bacteria foraging optimization algorithm based load frequency controller for interconnected power system," *International Journal of Electrical Power & Energy Systems*, vol. 33, no. 3, pp. 633-638, 2011.

[12] S. M. Abd-Elazim and E. S. Ali, "Load frequency controller design of a two-area system composing of PV grid and thermal generator via firefly algorithm," *Neural Computing and Applications*, vol. 30, no. 2, pp. 607-616, 2018.

[13] M. Farahani, S. Ganjefar, and M. Alizadeh, "PID controller adjustment using chaotic optimisation algorithm for multi-area load frequency control," *IET Control Theory & Applications*, vol. 6, no. 13, pp. 1984-1992, 2012.

[14] S. Padhy, S. Panda, and S. Mahapatra, "A modified GWO technique based cascade PI-PD controller for AGC of power systems in presence of plug in electric vehicles," *Engineering Science and Technology, an International Journal*, vol. 20, no. 2, pp. 427-442, 2017.

[15] M. Omar, M. Soliman, A. A. Ghany, and F. Bendary, "Optimal tuning of PID controllers for hydrothermal load frequency control using ant colony optimization," *International journal on electrical engineering and informatics*, vol. 5, no. 3, p. 348, 2013.

[16] C. K. Shiva, G. Shankar, and V. Mukherjee, "Automatic generation control of power system using a novel quasi-oppositional harmony search algorithm," *International Journal of Electrical Power & Energy Systems*, vol. 73, pp. 787-804, 2015.

[17] P. K. Pathak, S. Padmanaban, A. K. Yadav, P. A. Alvi, and B. Khan, "Modified incremental conductance MPPT algorithm for SPV- based grid- tied and stand- alone systems," *IET Generation, Transmission & Distribution*, vol. *16*, no. 4, pp. 776-791, 2022.

[18] D. Guha, P. K. Roy, and S. Banerjee, "Study of differential search algorithm based automatic generation control of an interconnected thermal-thermal system with governor dead-band," *Applied Soft Computing*, vol. 52, pp. 160-175, 2017.

[19] P. Hota and B. Mohanty, "Automatic generation control of multi source power generation under deregulated environment," *International Journal of Electrical Power & Energy Systems*, vol. 75, pp. 205-214, 2016.

[20] H. M. Hasanien and A. A. El-Fergany, "Symbiotic organisms search algorithm for automatic generation control of interconnected power systems including wind farms," *IET Generation, Transmission & Distribution*, vol. 11, no. 7, pp. 1692-1700, 2017.

[21] H. Gozde, M. C. Taplamacioglu, and I. Kocaarslan, "Comparative performance analysis of Artificial Bee Colony algorithm in automatic generation control for interconnected reheat thermal power system," *International Journal of Electrical Power & Energy Systems*, vol. 42, no. 1, pp. 167-178, 2012.

[22] D. Guha, P. K. Roy, and S. Banerjee, "Load frequency control of interconnected power system using grey wolf optimization," *Swarm and Evolutionary Computation*, vol. 27, pp. 97-115, 2016.

[23] S. P. Singh, T. Prakash, V. Singh, and M. G. Babu, "Analytic hierarchy process based automatic generation control of multi-area interconnected power system using Jaya algorithm," *Engineering applications of artificial intelligence*, vol. 60, pp. 35-44, 2017.

[24] A. D. Rosaline and U. Somarajan, "Structured H-Infinity controller for an uncertain deregulated power system," *IEEE Transactions on Industry Applications*, vol. 55, no. 1, pp. 892-906, 2018.

[25] K. Vrdoljak, N. Perić, and I. Petrović, "Sliding mode based load-frequency control in power systems," *Electric Power Systems Research*, vol. 80, no. 5, pp. 514-527, 2010.

[26] S. Sondhi and Y. V. Hote, "Fractional order PID controller for load frequency control," *Energy Conversion and Management*, vol. 85, pp. 343-353, 2014.

[27] X. Liu, Y. Zhang, and K. Y. Lee, "Coordinated distributed MPC for load frequency control of power system with wind farms," *IEEE Transactions on Industrial Electronics*, vol. 64, no. 6, pp. 5140-5150, 2016.

[28] A. M. Ersdal, L. Imsland, and K. Uhlen, "Model predictive load-frequency control," *IEEE Transactions on Power Systems*, vol. 31, no. 1, pp. 777-785, 2015.

[29] A. G. Haroun and Y. Li, "A novel optimized hybrid fuzzy logic intelligent PID controller for an interconnected multi-area power system with physical constraints and boiler dynamics," *ISA Transactions*, vol. 71, pp. 364-379, 2017.

[30] D. Sharma and S. Mishra, "Non-linear disturbance observer-based improved frequency and tie-line power control of modern interconnected power systems," *IET Generation, Transmission & Distribution*, vol. 13, no. 16, pp. 3564-3573, 2019.

[31] L. C. Saikia, Sukumar Mishra, Nidul Sinha, and J. Nanda., "Automatic generation control of a multi area hydrothermal system using reinforced learning neural network controller," *International Journal of Electrical Power & Energy Systems*, vol. 33, no. 4, pp. 1101-1108, 2011.

[32] A. Fathy, & Kassem, A. M., "Antlion optimizer-ANFIS load frequency control for multi-interconnected plants comprising photovoltaic and wind turbine," *ISA Transactions*, vol. 87, pp. 282-296, 2019.

[33] A. Latif, S. S. Hussain, D. C. Das, and T. S. Ustun, "Double stage controller optimization for load frequency stabilization in hybrid wind-ocean wave energy based maritime microgrid system," *Applied Energy*, vol. 282, pp. 116171, 2021.

[34] A. A. Abou El-Ela, R. A. El-Sehiemy, A. M. Shaheen, and A. E. G. Diab, "Design of cascaded controller based on coyote optimizer for load frequency control in multi-area power systems with renewable sources," *Control Engineering Practice*, vol. 121, pp. 105058, 2022.

[35] C. Pradhan, and C. N. Bhende, "Online load frequency control in wind integrated power systems using modified Jaya optimization," *Engineering Applications of Artificial Intelligence*, vol. 77, pp. 212-228, 2019.

[36] E. Çelik, "Performance analysis of SSA optimized fuzzy 1PD-PI controller on AGC of renewable energy assisted thermal and hydro-thermal power systems," *Journal of Ambient Intelligence and Humanized Computing*, pp. 1-20, 2022.

[37] M. Sharma, S. Dhundhara, Y. Arya, and S. Prakash, "Frequency excursion mitigation strategy using a novel COA optimised fuzzy controller in wind integrated power systems," *IET Renewable Power Generation*, vol. 14, no. 19, pp. 4071-85, 2020.

[38] A. Abazari, H. Monsef, B. Wu, "Coordination strategies of distributed energy resources including FESS, DEG, FC and WTG in load frequency control (LFC) scheme of hybrid isolated micro-grid," *International Journal of Electrical Power & Energy Systems*, vol. 109, pp. 535-547, 2019.

[39] E. Çelik, Öztürk, N., Arya, Y., & Ocak, C., "(1+ PD)-PID cascade controller design for performance betterment of load frequency control in diverse electric power systems " *Neural Computing and Applications*, pp. 1-24, 2021.

[40] P. K. Pathak, A. K. Yadav, A. Shastri & P.A. Alvi, "BWOA assisted PIDF-(1+ I) controller for intelligent load frequency management of standalone micro-grid," *ISA Transactions*, pp. 1-15, 2022. https://doi.org/10.1016/j.isatra.2022.06.010

[41] P. Dash, Saikia, L. C., & Sinha, N. , "Automatic generation control of multi area thermal system using Bat algorithm optimized PD–PID cascade controller," *International Journal of Electrical Power & Energy Systems*, vol. 68, pp. 364-372, 2015.

[42] R. Sivalingam, Chinnamuthu, S., & Dash, S. S., "A hybrid stochastic fractal search and local unimodal sampling based multistage PDF plus (1+ PI) controller for automatic generation control of power systems," *Journal of the Franklin Institute* vol. 354, no. 12, pp. 4762-4783., 2017.

[43] I. Naruei, & Keynia, F., "Wild horse optimizer: a new meta-heuristic algorithm for solving engineering optimization problems. Engineering with Computers," pp. 1-32, 2021.

[44] V. Hayyolalam, & Kazem, A. A. P., "Black widow optimization algorithm: a novel meta-heuristic approach for solving engineering optimization problems," *Engineering Applications of Artificial Intelligence,*, vol. 87, p. 103249, 2020.

[45] S. Jain and Y. V. Hote, "Design of generalised active disturbance rejection control for delayed systems: an application to load frequency control," *International Journal of Control*, vol. 94, no. 11, pp. 3146-3160, 2021.

[46] J. Morsali, K. Zare, and M. T. Hagh, "Applying fractional order PID to design TCSC-based damping controller in coordination with automatic generation control of interconnected multi-source power system," *Engineering Science and Technology, an International Journal*, vol. 20, no. 1, pp. 1-17, 2017.

[47] I. Pan, and S. Das, "Fractional order AGC for distributed energy resources using robust optimization," *IEEE Transactions on smart grid*, vol. 7, no. 5, pp. 2175-2186, 2015.

[48] F. N. Deniz, B. B. Alagoz, N. Tan, and D. P. Atherton, "An integer order approximation method based on stability boundary locus for fractional order derivative/integrator operators," *ISA Transactions*, vol. 62, pp. 154-163, 2016.

Appendix

Parameters of 2-area Reheat Thermal Power System [6]:

$R_i = 2.4$ Hz/puMW, $\beta_i = 0.425$Hz/$MW_{p.u.}$, $T_{Ti} = 0.3$ sec., $T_{Gi} = 0.08$sec., $T_{ri} = 10$ sec., $K_{ri} = 0.5$, $K_{PSi} = 120$Hz/puMW, $T_{PSi} = 20$ sec., $\alpha_{12} = -1$, $2\pi T_{12} = 0.545$ puMW/Hz, where, $i = 1, 2$.

Design of optimal cascade control approach for LFM of interconnected power system

Article history:
Received xxxxx
Received in revised form xxxxx
Accepted xxxxx
Available online xxxxx

Keywords:
Load frequency management
Fractional order cascade controller
Wild horse optimizer
Interconnected power system
Automatic generation control

ABSTRACT

In the present era, due to increasing power demand and complex power system structures having various load disturbances, a load frequency management (LFM) scheme is indispensable to provide uninterrupted power to consumers. This research deals with a fractional-order proportional derivative - (one + fractional order integrator) (FOPD-(1+FOI)) cascade controller as a novel control structure to ameliorate the performance of automatic generation control (AGC) for the LFM of interconnected power system (PS). The implementation of this controller is simple, and it connects the output of the FOPD controller to (1+FOI) controller, where area control error and power error are considered in the outer and inner feedback control loops, respectively. A maiden attempt of wild horse optimizer-assisted FOPD-(1+FOI) cascade controller for AGC of considered interconnected PS has been performed in this work. To benchmark the proposed control scheme, two areas reheat thermal PS with governor dead band and generation rate constraint nonlinearities are considered as the test bench. A vivid comparative analysis of six state-of-the-art control techniques is performed, and the results show the effectiveness of the proposed control scheme. Eigenvalues-based stability evaluation of considered interconnected PS in conjunction with the proposed controller is also performed. Finally, for the real power system implementation of the presented control scheme, a New England IEEE 39 test bus system is considered and analysed.

Abbreviations

ABC	Artificial bee colony
ACO	Ant colony optimization
AGC	Automatic generation control
ANFIS	Adaptive neuro-fuzzy inference system
ANN	Artificial neural network control
BWOA	Black widow optimization algorithm
COA	Coyote optimization algorithm
DE	Differential evolution
DSA	Dragonfly search algorithm
FA	Firefly algorithm
FO	Fractional order
FOPID	Fractional order PID
GA	Genetic algorithm
GDB	Governor dead band
GOA	Grasshopper optimization algorithm
GRC	Generation rate constraint
GSA	Gravitational search algorithm
hBFOA	Hybrid bacterial foraging optimization algorithm
HHO	Haris hawk optimization
IAE	Integral of absolute error
ISE	Integral of squared error
ITAE	Integral of time multiplied absolute error
ITSE	Integral of time multiplied squared error
LFD	Levy flight distribution
LFM	Load frequency management
MBA	Mine blast algorithm
MGWO	Modified grey wolf optimization
MVO	Multi-verse optimization
OS	Overshoot
PDF	Proportional-derivative with filter
PI-PD	Proportional integral-Proportional derivative
PID	Proportional-integral-derivative
PS	Power system
PSO	Particle swarm optimization
QOHS	Quasi-oppositional harmony search
SBL	Stability boundary locus
SSA	Salp swarm algorithm
TSA	Tunicate swarm algorithm
US	Undershoot
WHO	Wild horse optimizer

1. Introduction

1.1 Background

Due to racing power demand in today's world, including PS size spurt, complexity, and interconnected PS network, it is a very challenging task to provide secure, uninterrupted, and stable power via proper power flow management [1]. The power demand is continuously fluctuating in nature, resulting in transient deviations in frequency and tie-line power flow of the entire PS [2-4]. Various control areas are connected to a PS network. From the electrical utility point of view, for stable and reliable operation, power generated in each control area must be equal to the power demands, and total losses occurred; as well as tie-line and deviation of frequency from reference should fall within permissible close to zero limits. To this end, noteworthy and rapid development has been seen in the LFM area because it is impossible to maintain the balance among demands-generations without supplementary control action [5, 6]. In real-time, AGC is the control action

that stabilizes the demand-generation balance and maintains the frequency deviations of the entire PS within permissible limits. In other words, LFM force the synchronous generator units to regulate their generations to meet the load demands. In view of the above-mentioned discussion, an enhanced and effective control scheme is an unavoidable requirement for the LFM of PSs. Moreover, for the purpose of engineering commissioning, the practical potential and suitability of an LFM control scheme in a real-time implementation is a much-needed feature [7-9].

1.2 Literature Review

From the comprehensive literature survey, it is pointed out that there are enormous highly cited works in the area of LFM present in the last few decades. Every article is endeavoring for further enhancement. In Ref. [2], PIDD2 controller based on the internal model control and worst-case plant selection scheme is proposed for the LFM of time-delayed interconnected PS. A novel performance index based on a hybrid peak area for the AGC of interconnected PS is briefed in [3]. In this, the authors have performed a comparative analysis of the proposed performance index with the existing indices. A fuzzy logic-based adaptive LFM of renewable energy shared standalone microgrid is demonstrated in [5]. In this, a fuzzy observer is used to extract the power from wind turbine generator, and an improved incremental conductance scheme is used to harvest maximum power from the solar. For the real power system implementation of the proposed control scheme, authors have considered a New England IEEE 39 test bus system. A fuzzy logic-based fractional variant of the PID controller is used to investigate the AGC performance of interconnected PS [7]. Few articles that are recently published employing PI/PID based controllers are (hBFOA-PSO) [10], BFOA [11], FA [12], lozi-map based chaotic algorithm [13], MGWO [14], ACO [15], QOHS [16], GA [17], DSA [18], DE [19], symbiotic organisms search [20], ABC [21], GWO tuned PI/PID controllers [22], and Jaya algorithm assisted PID with low pass filter [23]. To palliate control mechanism, other advanced control techniques based on H-infinity [24], sliding mode control [25], fractional calculus theory [26], model predictive control [27, 28], fuzzy logic approach [29], nonlinear disturbance observer [30], ANN [31], and ANFIS [32] are presented in the relevant field. A double-stage PI-(1+PD) controller is designed via a GOA scheme for the LFM of wind-ocean-based maritime PS in [33]. A comparative analysis among PID, PIDF, and PI-(1+PD) tuned via GA, PSO, FA, and GOA is performed, and the obtained results revealed the superior performance of the proposed controller. Design consideration of the cascade controller for the frequency control of multi-area PS based on COA is briefed in [34]. The simulation results revealed the proposed cascade PDF-PI controller's superior and robust dynamic performance under parametric uncertainties. The maximum frequency deviations under the worst condition are not exceeding 0.4% for the proposed control scheme. Online LFM in wind integrated PSs via modified jaya optimization is described in [35]. The performance assessment of SSA tuned intelligent fuzzy 1PD-PI controller for the AGC of renewable rich multi-area PS is presented in Ref. [36]. In this, author has designed a cascade control approach for the frequency control with the stability evaluation of the proposed technique. A frequency deviation mitigation technique via COA tuned fuzzy controller under wind integrated PS is briefed in [37]. A frequency control mechanism of distributed energy resources based on coordinated strategies is revealed in [38]. In this, small signal dynamic models for renewable energy sources are introduced in standalone microgrid. Design of active disturbance rejection based LFM of time delayed PS is demonstrated in [45]. Fraction order controller is designed for the AGC of multi area PS in Refs. [46, 47].

The PS works under various uncertainty conditions due to stochastic load demands, inherent nonlinearities, communication delays, and continuous variation in its structure. Though the intelligent algorithms tuned conventional controllers, as mentioned above, show good performance, their performance may greatly affect in regards to longer settling time and larger oscillations. Moreover, the output of the traditional controllers optimized for a specific point will worsen with changing operating conditions of the system. The fractional and cascade concept of controller design is much appreciated for its enhanced disturbance rejection capability before it is transmitted to other sections of the system and as underlined by researchers. A cascade control structure has the potential to provide enhanced performance to the traditional controller [39]. In this regard, MGWO tuned PI-PD cascade controller [14], BWOA tuned PIDF-(1+I) controller [40], bat algorithm optimized PD-PID cascade controller [41], DE based multi-stage PDF plus (1+PI) controller [42] are briefed for LFM of various PSs.

From the above-mentioned vivid literature review, the critical observations are; (1) the implementation of the metaheuristic approach on the fuzzy-logic, ANN and ANFIS, makes the system very complex, (2) designed controllers in the literature are just standard feedback control-based approach, and (3) there is always a scope to implement robust, advanced, and recently invented metaheuristic approach for the LFM of the power system.

1.3 Motivation and Contributions

The system responses of these cascade controllers are showing worth appreciating control effort in the area of interest. However, as per the best knowledge of the authors' results obtained in these works have some space for enhancement while considering the time domain specifications such as OS, US, rise time, and settling time, as well as error constants such as IAE, ITAE, ISE, and ITSE. The presented study revisits LFM by introducing a new factional and cascade controller named FOPD-(1+FOI), whose benchmarking is not yet investigated so far. In view

of the inspected literature, various nature-inspired optimizations are implemented in LFM studies for the purpose of proper gain tuning and to obtain the possible outcome from the controllers. WHO, a recently invented metaheuristic algorithm proposed by Iraj Naruei and Farshid Keynia (2021) [43] has proved its efficacy over GA, PSO, GWO, MVO, TSA, LFD, SSA, GSA, and HHO in various problems such as [43]; process synthesis and design, heat exchange design, two-reactor problem, tension/compression spring design, step-cone pully, three bar truss design, rolling-element bearing, and gas transmission compressor design, so it is considered for the LFM of the considered interconnected PS. A vivid comparative analysis of the proposed LFM controller design in terms of time-domain indices and error rates is performed with other metaheuristics like; GWO, MBA, MGWO, and recently invented BWOA [44], and other control structures like; FOPID, PI-PD, and PID. Moreover, a stability evaluation of the proposed LFM scheme is also performed in this work. For the stability evaluation, the fractional orders are approximated into their respective full-order terms via the SBL method [48]. In comparison with the existing literature, the significant contributions of the work are as follows:

1) Design of WHO tuned FOPD-(1+FOI) fractional cascade controller for LFM of two areas PS and its superiority has been established over designed FOPID, PI-PD, and PID controllers.
2) Performance assessment of WHO is verified over MBA, GWO, and BWOA concerning minimum fitness value, cost-effectiveness, and convergence rate.
3) Benchmarking of the proposed controller's robustness concerning parametric uncertainties and load disturbances.
4) Eigenvalues-based stability evaluation of the proposed LFM scheme.
5) For real power system validation, the proposed LFM technique is implemented on New England IEEE 39 test bus system.

The rest of the paper is documented as; Section 2 deals with the studied PS model, and Section 3 describes the vivid design consideration of the proposed controller. A vivid description of WHO is presented in Section 4, results and discussion with stability evaluation and real power system implementation are revealed in Section 5. The final concluding remark is given in Section 6.

2. Power System Model Under Investigation

A two-area interconnected reheat thermal PS is investigated and revealed in Fig. 1, and each PS control area has a load of 2000 MW. The reheat thermal PS with GDB and GRC has been comprehensively captivated in the AGC literature [2, 3] and [6, 8]. The generation speed is restricted due to the practical moderation of thermal and mechanical activities shown by GRC. On the other hand, GDB is a measure of continuous speed variation in which there is no deviation in the position of the valve. In order to conduct a real-time investigation on AGC in the presence of nonlinearities, GDB and GRC must be considered. In Fig. 1, the various components are as: area control error (ACE), governor regulation (R), frequency biasing (β), controller output (ΔP_c), turbine time constant (TC) (T_T), governor TC (T_G), reheater TC (T_r), reheater gain (K_r), change in load (ΔP_D), power error P_e, turbine power (ΔP_g), PS gain (K_{PS}), PS TC (T_{PS}) and area capacity ratio (α_{12}). Moreover, ΔF_i (change in frequency), $\Delta Ptie_{ij}$ (change in tie-line power), and T_{ij} (synchronizing coefficient). The detailed parameters of the considered two-area reheat thermal PS are provided in Appendix.

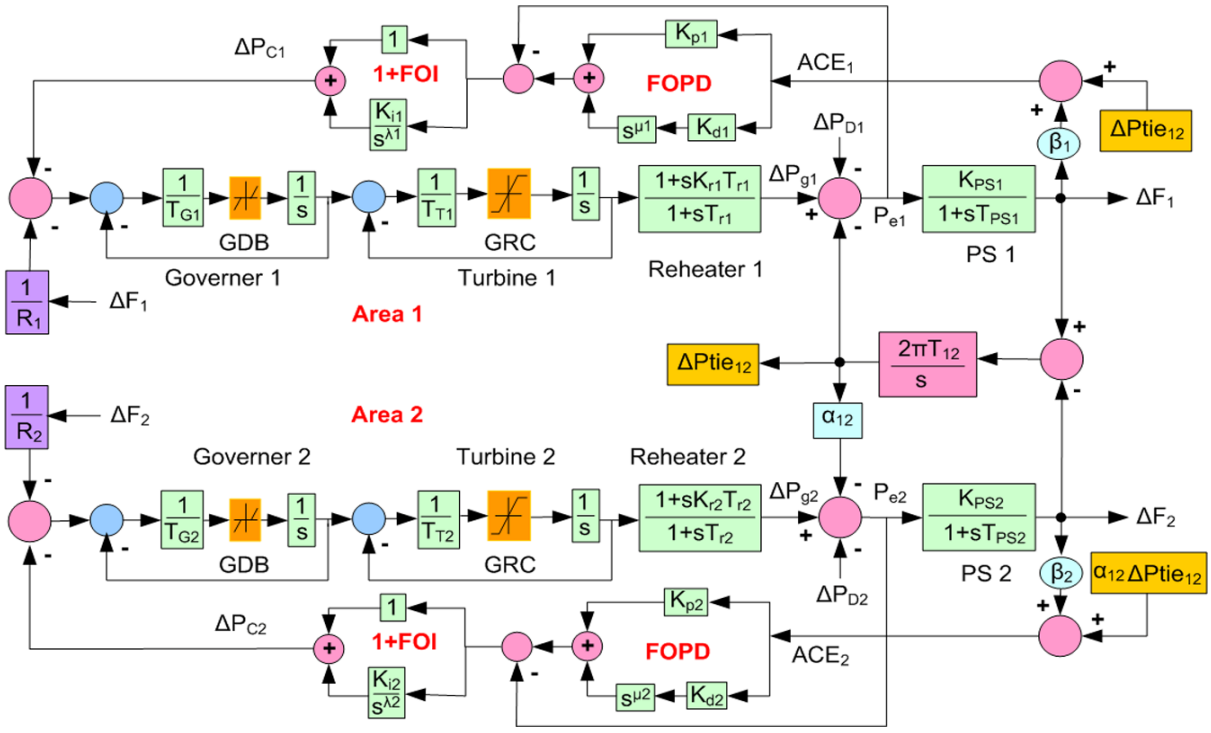

Fig. 1 Two-areas reheat thermal PS with FOPD-(1+FOI) cascade control

The generalized dynamics of multiarea PS in the form of a transfer function (TF) are described as follows [2]:

Governor $TF = G_{G,i}(s) = \frac{1}{(1+sT_{Gi})}$ (1)

Reheated turbine $TF = G_{T,i}(s) = \frac{1}{(1+sT_{Ti})}\frac{(1+sK_{ri}T_{ri})}{(1+sT_{ri})}$ (2)

PS $TF = G_{PS,i}(s) = \frac{K_{PSi}}{(1+sT_{PSi})}$ (3)

where $i = 1, 2 \ldots . . N$.

3. Proposed Controller Design

3.1 Fractional order (FO) calculus

The generalized form of integer order calculus is the FO calculus that converts the integer-order differential and integral operators to the FO. ${}_{A}\mathrm{Q}_{t}^{\bar{\alpha}}$ is the fractional operator responsible for the transform. Based on the sign of $\bar{\alpha}$, the differentiation or integration operation is decided. The modeling of the fractional operator is as follows [46]:

$${}_{A}\mathrm{Q}_{t}^{\bar{\alpha}} = \begin{cases} \frac{d^{\bar{\alpha}}}{dt^{\bar{\alpha}}}, & \bar{\alpha} > 1 \\ 1, & \bar{\alpha} = 0 \\ \int_{\bar{\alpha}}^{t}(dt)^{\bar{\alpha}}, & \bar{\alpha} < 1 \end{cases} \quad (4)$$

There is various literature available for the definitions of the FO functions. A few definitions are the Grunwald-Letnikov (G-L) definition, Riemann-Liouville (R-L) definition, and the Caputo definition [46].

The most used definition is R-L, which is as follows [46]:

$${}_{A}\mathrm{Q}_{t}^{\bar{\alpha}} = \frac{1}{\Gamma(k-\bar{\alpha})}\frac{d^{k}}{dt^{k}}\int_{\bar{\alpha}}^{t}\frac{x(\tau)}{(t-\tau)^{1-(k-\bar{\alpha})}}d\tau \quad (5)$$

where, $\Gamma(\cdot)$ is the Euler's gamma function, and k is an integer $k-1 < \bar{\alpha} \leq k$. Before using the FO controller in real or simulation applications, it is required the approximation of FO differentiators and integrators with corresponding integer-order counterparts. Moreover, the FO differentiators and integrators are infinite-dimensional in nature, so before putting them into practice, must be band limited. To band limit them, various approximation schemes are available such as Matsuda approximation, Carlson approximation, Oustaloup's recursive approximation, and Crone approximation [47]. In this proposed work, Oustaloup's recursive approximation is employed to realize FO controllers within the frequency range of ($\omega_l = 0.001$, $\omega_u = 1000$) rad/s. Using this, FO differentiator and integrator are approximated via recursive distribution of zeroes and poles as:

$$s^{\bar{\alpha}} = M\prod_{k=1}^{K}\frac{1+\left({}^{s}/_{\omega_{z,k}}\right)}{1+\left({}^{s}/_{\omega_{p,k}}\right)} \quad (6)$$

Frequencies of zeros and poles are:

$$\begin{cases} \omega_{z1} = \omega_l\sqrt{\eta} \\ \omega_{z,k} = \omega_{z,k}\varepsilon, \ \ k = 1,2,3, \ldots \ldots, K \\ \omega_{z,k+1} = \omega_{p,k}\sqrt{\eta}, \ \ k = 1,2,3, \ldots \ldots, K-1 \\ \varepsilon = \left(\frac{\omega_u}{\omega_l}\right)^{{}^{\bar{\alpha}}/_{K}} \\ \eta = \left(\frac{\omega_u}{\omega_l}\right)^{{}^{(1-\bar{\alpha})}/_{K}} \end{cases} \quad (7)$$

In this work, the authors have utilized the fractional-order modeling and control (FOMCON) toolbox for the designing of the proposed FO controller.

3.2 Cascade controller

The key feature of the cascade controller is to mitigate the impact of disturbance propagation through another part of the system since it gives an extra feedback path, i.e., sensor for restricting and reducing disturbance quickly before the final output [34]. It consists of two loops, as revealed in Fig. 2.

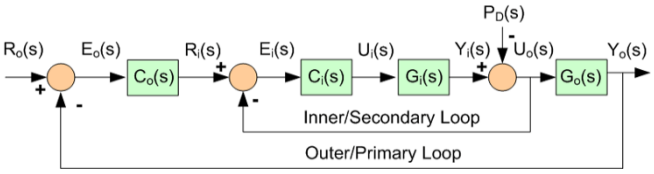

Fig. 2 Structure of proposed cascade controller

The outer loop is considered the primary loop that carries $Y_o(s)$ as the controlled output. Its gain $G_o(s)$ is affected by the power demand $P_D(s)$ and expressed as:

$$Y_o(s) = G_o(s)U_o(s) = G_o(s)\big(Y_i(s) - P_D(s)\big) \quad (8)$$

where, $U_o(s)$ is the input signal to $G_o(s)$, which is equivalent to the inner loop's processed output $Y_i(s)$. The outer loop's controller is $C_o(s)$, which will supervise $Y_o(s)$ to receive a reference signal $R_o(s)$. The inner loop is considered the secondary loop and will process the inner loop's gain $G_i(s)$ and formulated as:

$$Y_i(s) = G_i(s)U_i(s) \quad (9)$$

where, $U_i(s)$ is the input signal to the $G_i(s)$ and $C_i(s)$ is the controller for the inner loop. Its objective is to reduce the inner process gain deviations impact. The complete transfer function for the cascade control is revealed as follows:

$$Y_o(s) = \left[\frac{G_o(s)G_i(s)C_o(s)C_i(s)}{1+G_o(s)C_o(s)+G_o(s)G_i(s)C_o(s)C_i(s)}\right]R_o(s) - \left[\frac{G_o(s)}{1+G_o(s)C_o(s)+G_o(s)G_i(s)C_o(s)C_i(s)}\right]P_D(s) \quad (10)$$

In this work, the proposed cascade controller is FOPD-(1+FOI), where the primary/outer loop controller $C_o(s)$ is FOPD, and the inner loop controller $C_i(s)$ is (1+FOI), as depicted in Fig. 1. The two controllers can be described in the generalized form as:

$$C_{o,i}(s) = K_{pi} + K_{di}s^{\mu i} \quad (11)$$

$$C_{i,i}(s) = 1 + \frac{K_{ii}}{s^{\lambda i}} \quad (12)$$

where i=1 for area-1 and i=2 for area-2, and K_{pi} is the proportional gain, K_{di} is differential gain, μi is differential fractional order, K_{ii} is integral gains, and λi is integral fractional order. Due to the cascade connection of two controllers, it obtains the property of disturbance rejection before they outspread to another system. From Fig. 1, the resulting equations for area-1 are as:

$$\Delta F_1 = G_{PS,1}(s)P_{e1} \quad (13)$$

$$P_{e1} = \Delta P_{g1} - \Delta Ptie_{12} - \Delta P_{D1} \quad (14)$$

$$\Delta P_{g1} = G_{G,1}(s)G_{T,1}(s)\left(-\Delta P_{c1} - \frac{1}{R_1}\Delta F_1\right) \quad (15)$$

$$\Delta P_{c1} = C_{i,1}(s)\big(C_{o,1}(s) * ACE_1 - P_{e1}\big) \quad (16)$$

$$ACE_1 = \beta_1 \Delta F_1 + \Delta Ptie_{12} \quad (17)$$

$$\Delta Ptie_{12} = \frac{2\pi T_{12}}{s}(\Delta F_1 - \Delta F_2) \quad (18)$$

To establish the independent relations for area-1, considering the $\Delta F_2 = 0$ in (18), and from (13)-(18), yield (19). Similarly, the decoupled equation for area-2 is derived and represented by (20). To obtain the optimal controller performance, a total of ten parameters in both areas of PS must be optimized. WHO is chosen for the simultaneous optimization of these parameters. The optimized value of any controller depends on the appropriate objective function (J).

$$\Delta F_1 = -\left[\frac{G_{PS,1}(s)}{1+\frac{2\pi T_{12}}{s}G_{PS,1}(s)-G_{G,1}(s)G_{T,1}(s)C_{i,1}(s)+G_{G,1}(s)G_{T,1}(s)G_{PS,1}(s)C_{i,1}(s)C_{o,1}(s)\left(\beta_1+\frac{2\pi T_{12}}{s}\right)+\frac{G_{G,1}(s)G_{T,1}(s)G_{PS,1}(s)}{R_1}}\right]\Delta P_{D1} \quad (19)$$

$$\Delta F_2 = -\left[\frac{G_{PS,2}(s)}{1+\frac{2\pi T_{12}}{s}G_{PS,2}(s)-G_{G,2}(s)G_{T,2}(s)C_{i,2}(s)+G_{G,2}(s)G_{T,2}(s)G_{PS,2}(s)C_{i,2}(s)C_{o,2}(s)\left(\beta_2+\frac{2\pi T_{12}}{s}\right)+\frac{G_{G,2}(s)G_{T,2}(s)G_{PS,2}(s)}{R_2}}\right]\Delta P_{D2} \quad (20)$$

Different types of J have been utilized in the literature as mentioned below:

$$(\text{ISE}) = \int_0^t \{(\Delta F_1)^2 + (\Delta F_2)^2 + (\Delta Ptie_{12})^2\}dt \quad (21)$$

$$(\text{ITSE}) = \int_0^t t\{(\Delta F_1)^2 + (\Delta F_2)^2 + (\Delta Ptie_{12})^2\}dt \quad (22)$$

$$(\text{IAE}) = \int_0^t \{|\Delta F_1| + |\Delta F_2| + |\Delta Ptie_{12}|\}dt \quad (23)$$

$$(\text{ITAE}) = \int_0^t t\{|\Delta F_1| + |\Delta F_2| + |\Delta Ptie_{12}|\}dt \quad (24)$$

where t is the simulation time, ΔF_1, ΔF_2 and ΔPtie_{12} are the responses against step load perturbation (SLP). Controlled response with damped oscillations and less settling time are obtained while dealing with ITAE objective function, and it is implemented in LFM studies very frequently [6], [33-35] compared to other variants; hence, it is considered in the presented study. The design of the controller is a constrained tuning task, where the bounds parameter of the controller works as a constraint. Hence, lessen J considering to:

$$\begin{Bmatrix} K_{p1}^{min} \le K_{p1} \le K_{p1}^{max} \\ K_{d1}^{min} \le K_{d1} \le K_{d1}^{max} \\ K_{i1}^{min} \le K_{i1} \le K_{i1}^{max} \\ K_{p2}^{min} \le K_{p2} \le K_{p2}^{max} \\ K_{d2}^{min} \le K_{d2} \le K_{d2}^{max} \\ K_{i2}^{min} \le K_{i2} \le K_{i2}^{max} \\ \mu 1^{min} \le \mu 1 \le \mu 1^{max} \\ \mu 2^{min} \le \mu 2 \le \mu 2^{max} \\ \lambda 1^{min} \le \lambda 1 \le \lambda 1^{max} \\ \lambda 2^{min} \le \lambda 2 \le \lambda 2^{max} \end{Bmatrix} \quad (25)$$

These ten parameters are obtained via running WHO to enhance the complete system performance of the proposed interconnected PS.

4. Wild Horse Optimizer (WHO)

The behavior of non-territorial horses is the motivation for this optimization technique which was proposed in 2021 [43]. WHO consists of five key steps; in the first step initial population is created, and horse groups are formed with the selection of leaders; mating and grazing of horses is the second step; in the third step, the groups are leaded by the leader (stallion); the process of exchange and selection of leaders have occurred in the fourth step, and in the final step, the best solution is obtained. For proper communication, stallions are located near the mares, and mating occurs at any time. Generally, foals are started grazing in the initial week and have less rest time as they become older. The random initial population is considered as follows:

$$(\vec{x}) = \{\vec{x}_1, \vec{x}_2, \vec{x}_3 \dots\dots\dots\dots\dots, \vec{x}_n\} \quad (26)$$

The process of evaluation of this random population is performed via the target function. The target function is evaluated as:

$$(\vec{O}) = \{O_1, O_2, O_3 \dots\dots\dots\dots\dots O_n\} \quad (27)$$

Firstly, the population is divided into various groups. The number of groups is $G = [n \times ps]$, where n is the number of members and ps is the percentage of stallions, and it is the control parameter in this algorithm. This population division is revealed in Fig. 3.

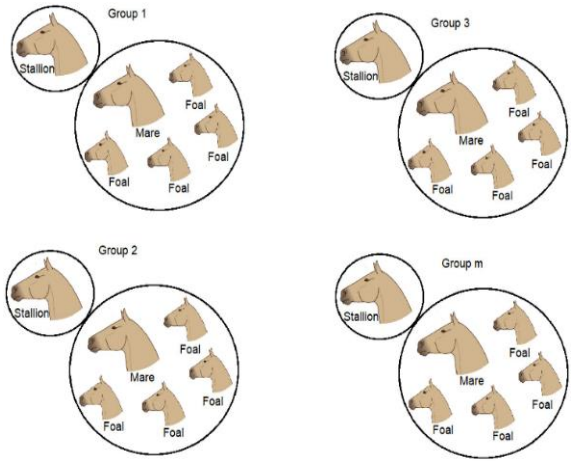

Fig. 3 Formation of horse groups in initial population [43]

To obtain the grazing behavior, the stallion is placed in the center of the grazing area, and other members search around the center. The grazing behavior is simulated as:

$$\bar{X}_{i,G}^{j} = 2Z\cos(2\pi RZ) \times \left(Stallion^{j} - X_{i,G}^{j}\right) + Stallion^{j} \quad (28)$$

where, $\bar{X}_{i,G}^{j}$ is the new position of group member while grazing, the current position of foal or mare is $X_{i,G}^{j}$, the position of the group leader is $Stallion^{j}$, R is uniform distribution in $[-2, 2]$, Z is the adaptive mechanism calculated as:

$$P = \vec{R}_1 < TDR; \quad IDX = (P == 0); \quad Z = R_2 \Theta IDX + \vec{R}_3 \Theta(\sim IDX) \quad (29)$$

P is a vector with values 0 and 1, $\vec{R}_1, R_2$ and $\vec{R}_3$ are random vectors with [0,1], IDX is the index of a random vector $\vec{R}_1$ satisfying $(P == 0)$, TDR is an adaptive parameter with an initial value 1 and decreased to 0 as the execution of the algorithm starts as:

$$TDR = 1 - iter \times \left(\frac{1}{maxiter}\right) \quad (30)$$

where, $iter$ and $maxiter$ are the current and maximum iterations. One of the important behavior of horses is separating foals from the group and mating them while compared with other animals. The mating process of horses is simulated as:

$$X_{G,K}^{p} = Crossover\left(X_{G,i}^{q}, X_{G,i}^{z}\right) \quad i \neq j \neq k, p = q = end,$$
$$Crossover = Mean \tag{31}$$

In group k, the position of horse p is $X_{G,K}^{p}$ and gives it a place who have to leave group i and j. The position of foal q is $X_{G,i}^{q}$ from group i, it mated with a horse (z) with position $\left(X_{G,i}^{z}\right)$, which leaves group j. The group leader has the capability to lead the group to an appropriate area (water hole), and this process is simulated by:

$$\overline{Stallion_{G_i}} = \begin{Bmatrix} 2Z\cos(2\pi RZ) \times \left(WH - Stallion_{G_i}\right) + WH \;\; if R_3 > 0.5 \\ 2Z\cos(2\pi RZ) \times \left(WH - Stallion_{G_i}\right) - WH \;\; if R_3 \leq 0.5 \end{Bmatrix} \tag{32}$$

$$\overline{Stallion_{G_i}} = \begin{Bmatrix} X_{G,i} & if\cos t\left(X_{G,i}\right) < \cos t\left(Stallion_{G_i}\right) \\ Stallion_{G_i} & if\cos t\left(X_{G,i}\right) > \cos t\left(Stallion_{G_i}\right) \end{Bmatrix} \tag{33}$$

where, the next position of leader is $\overline{Stallion_{G_i}}$ of the group i, the position of water hole is WH, and the current position of leader is $Stallion_{G_i}$ of the group i. The flowchart of the WHO scheme is shown in Fig. 4.

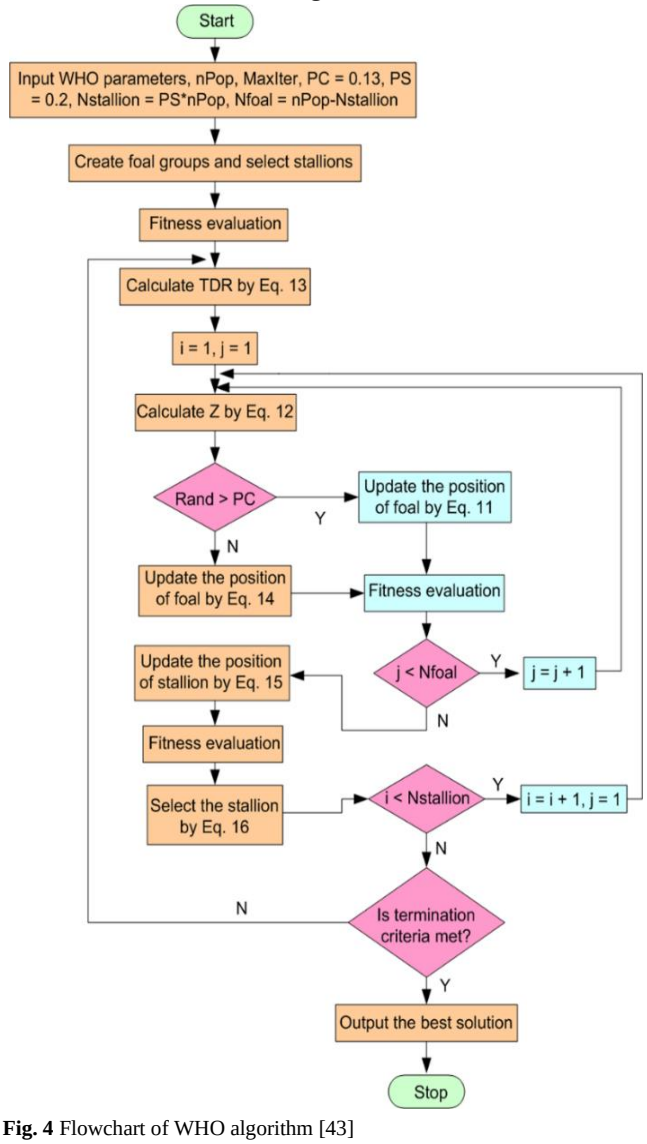

Fig. 4 Flowchart of WHO algorithm [43]

5. Results and Discussion

5.1 Test case-1 with SLP of 10% in area-1

The proposed WHO:FOPD-(1+FOI) fractional cascade controller is implemented on an interconnected reheat thermal PS. A state-of-the-art of five optimization techniques as MBA, GWO, MGWO, BWOA, and WHO, and four different types of controllers as PID, FOPID, PI-PD, FOPD-(1+FOI) for the LFM have been briefed. To benchmark the superior performance of fractional cascade controller, the convergence rates of WHO:PID, WHO:FOPID, WHO:PI-PD, and WHO:FOPD-(1+FOI) are depicted in Figs. 5(a)-(d), respectively, and analyzed in Table 1.

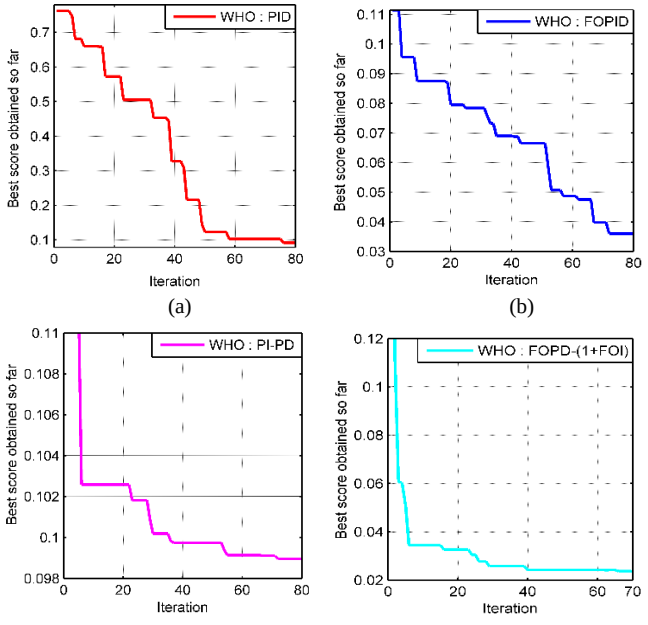

Fig. 5 Convergence of WHO tuned (a) PID, (b) FOPID, (c) PI-PD and (d) FOPD-(1+FOI)

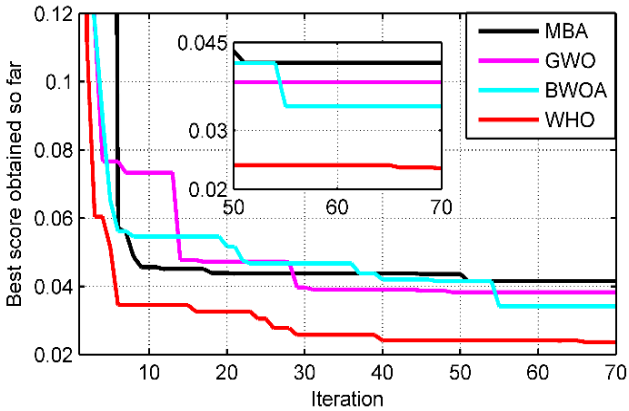

Fig. 6 Convergence rate of various metaheuristics for FOPD-(1+FOI) controller

Table 1: Convergence analysis of all designed control schemes

Techniques	Iterations	Minimum *J*
WHO:PID	77	0.1
WHO:FOPID	72	0.038
WHO:PI-PD	75	0.099
MBA:FOPD-(1+FOI)	53	0.0415
GWO:FOPD-(1+FOI)	49	0.0395
BWOA:FOPD-(1+FOI)	56	0.0366
Proposed	**40**	**0.0234**

In the case of WHO:PID the best score is obtained after 77 iterations with a minimum J of 0.1; for WHO:FOPID the best score is obtained after 72 iterations with a minimum J of 0.038; for WHO:PI-PD the best score is obtained after 75 iterations with a minimum J of 0.099, while for the proposed WHO:FOPD-(1+FOI) controller the best score is obtained after 40 iterations with minimum J of 0.0234. So, from the above-mentioned analysis and results revealed in Figs 5(a)-(d) it is concluded that the proposed fractional cascade controller is fast enough and cost-effective in comparison to full order controller, fractional-order controller, and full order cascade controller. Fig. 6 and Table 1 have revealed the convergence of different meta-heuristics applied to FOPD-(1+FOI) controller. It is noted that the best score with faster convergence and cost-effectiveness is obtained in the case of the proposed WHO scheme with a minimum J of 0.0234 in comparison to MBA, GWO, and BWOA. An SLP of 10% is provided in area-1, and the responses as ΔF_1, ΔF_2 and $\Delta Ptie$ via the implementation of various control schemes are presented in Figs 7(a)-(c), respectively.

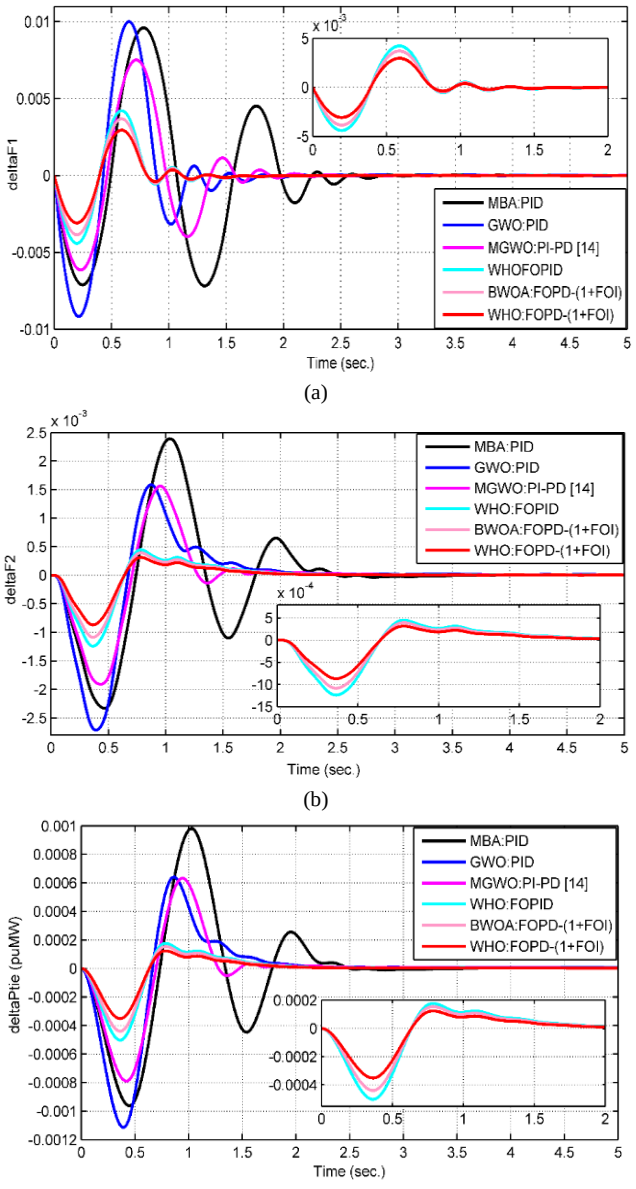

Fig. 7 Performance of controllers with SLP of 10% in area 1 (a) ΔF_1 (Hz) (b) ΔF_2 (Hz), and (c) $\Delta Ptie$

The maximum OS in ΔF_1 is 0.01 Hz (GWO:PID) and minimum for the proposed WHO:FOPD-(1+FOI) controller (0.0023 Hz). The maximum OS of 2.4×10^{-3} Hz is obtained for ΔF_2 in the case of MBA:PID and minimum are noted for the proposed controller as 0.24×10^{-3}. While analyzing the US, the maximum US in ΔF_1 is 0.0097 Hz (GWO:PID), and the minimum US is 0.0029 Hz obtained for the proposed control scheme. As depicted in Fig. 7(b) and Table 2, the USs in ΔF_2 are 0.0023 Hz, 0.0028 Hz, 0.00192 Hz, 0.00125 Hz, 0.0011 Hz, and 0.0008 Hz for MBA:PID, GWO:PID, MGWO:PI-PD, WHO: FOPID, BWOA:FOPD-(1+FOI) and proposed controller respectively. Moreover, the minimum US of the order of 0.00035 is obtained for WHO:FOPD-(1+FOI) controller while dealing with the response of $\Delta Ptie$. While analyzing the settling time (t_s) of ΔF_1, the t_s of 3.3 sec., 2.3 sec., 2.4 sec., 1.5 sec., 1.3 sec., and 1.3 sec. for MBA:PID, GWO:PID, MGWO:PI-PD, WHO: FOPID, BWOA: FOPD-(1+FOI) and proposed controller respectively is obtained. The maximum t_s are 3.55 sec., and 3 sec. for ΔF_2 and $\Delta Ptie$ respectively for MBA:PID controller, and the minimum is noted for the proposed WHO:FOPD-(1+FOI) controller as mentioned in Table 2. Further while dealing with the error constants for ΔF_1, ΔF_2 and $\Delta Ptie$, the minimum of IAE, ITAE, ISE, and ITSE is noted for the proposed controller, and the maximum is noted for MBA:PID controller.

5.2 Test case-2 with SLP of 20% in area-1 and SLP of 10% in area-2

In this section, the analysis of the performance of all applied controllers for LFM is evaluated. Figs. 8(a)-(c) show the response of ΔF_1, ΔF_2 and $\Delta Ptie$ and vivid comparative analysis of the controller performance is given in Table 3.

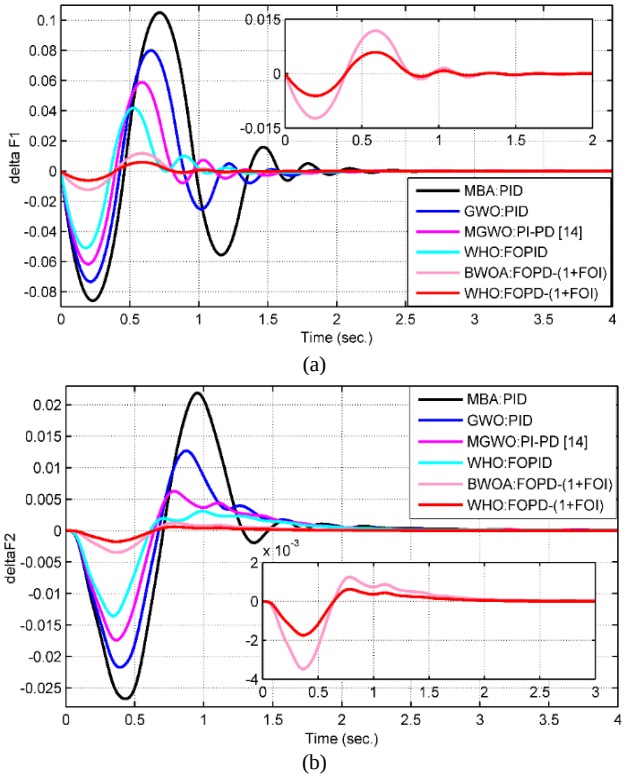

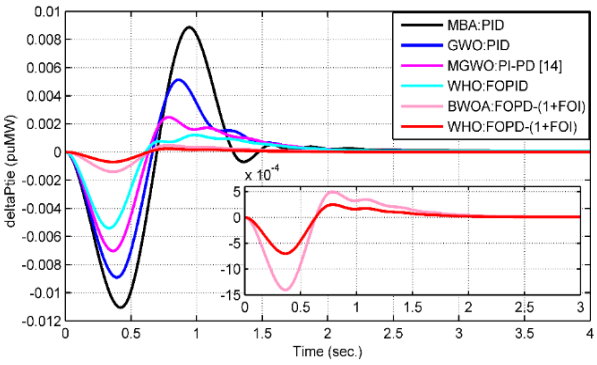

(c)

Fig. 8 Performance of controllers with SLP of 20% in Area-1 and SLP of 10% (a) ΔF_1 (Hz), (b) ΔF_2 (Hz), and (c) $\Delta Ptie$

The maximum OS (0.11 Hz) of ΔF_1 is obtained in the case of MBA-PID, and the minimum OS (0.0065 Hz) is for the proposed controller. For ΔF_2 OSs are 0.024 Hz, 0.013 Hz, 0.0065 Hz, 0.017 Hz, 0.0013 Hz, and 0.0008 Hz for MBA:PID, GWO:PID, MGWO:PI-PD, WHO:FOPID, BWOA:FOPD-(1+FOI) and proposed controller respectively, while the USs are 0.028 Hz, 0.022 Hz, 0.018 Hz, 0.014 Hz, 0.0036 Hz, and 0.0018 Hz respectively for the same applied controller. While dealing with the $\Delta Ptie$, the maximum OS and US are 0.009 and 0.011 for MBA:PID, and the minimum OS and US are 0.0002 and 0.0006 for the proposed controller. From Figs. 8(a)-(c) and Table 3, the t_s (ΔF_1) are 2.4 sec., 2 sec., 1.9 sec., 1.8 sec., 1.3 sec., and 1.2 sec., the t_s (ΔF_2) are 2.6 sec., 2.5 sec., 2.3 sec., 2.4 sec., 2.2 sec., 2 sec. for MBA:PID, GWO:PID, MGWO:PI-PD, WHO:FOPID, BWOA:FOPD-(1+FOI), and proposed controller respectively. In the case of tie-line flow the t_s are, 3.2 sec., 2.7 sec., 2.4 sec., 2.2 sec., 2 sec., 2 sec. for MBA:PID, GWO:PID, MGWO:PI-PD, WHO:FOPID, BWOA:FOPD-(1+FOI) and WHO:FOPD-(1+FOI) controllers respectively. While dealing with the error constants, the minimum of IAE, ITAE, ISE, and ITSE is obtained for the proposed controller, and the maximum IAE, ITAE, ISE, and ITSE is obtained for MBA:PID controller for ΔF_1, ΔF_2 and $\Delta Ptie$ as tabulated in Table 3.

Table 2: Comparative analysis of different control schemes for SLP of 10% in area-1

SLP of 10% in area-1							
Performance Indices		**MBA: PID**	**GWO: PID**	**MGWO: PI-PD [14]**	**WHO: FOPID**	**BWOA: FOPD-(1+FOI)**	**WHO: FOPD-(1+FOI)**
Overshoot (OS)	ΔF_1(Hz)	0.00950	0.0100	0.0078	0.00410	0.0038	**0.0023**
	ΔF_2(Hz)	0.00240	0.00152	0.00151	0.00048	0.00046	**0.00024**
	$\Delta Ptie$(puMW)	0.00100	0.00062	0.00062	0.00019	0.00017	**0.0001**
Undershoot (US)	ΔF_1(Hz)	0.00770	0.0097	0.00610	0.0043	0.0039	**0.0029**
	ΔF_2(Hz)	0.00230	0.0028	0.00192	0.00125	0.0011	**0.00080**
	$\Delta Ptie$(puMW)	0.00095	0.0011	0.0008	0.0005	0.00045	**0.00035**
Rise time (t_r) (sec.)	ΔF_1	0.50000	0.4500	0.4700	0.4000	0.4000	**0.4000**
	ΔF_2	0.80000	0.7000	0.7500	0.6500	0.6500	**0.6500**
	$\Delta Ptie$	0.75000	0.7100	0.7300	0.6200	0.6200	**0.6200**
Settling time (t_s) (sec.)	ΔF_1	3.3000	2.3000	2.4000	1.5000	1.3000	**1.3000**
	ΔF_2	3.5500	2.4000	2.3000	2.0000	1.9000	**1.9000**
	$\Delta Ptie$	3.000	3.0000	2.4000	1.9000	1.9000	**1.9000**
ΔF_1	IAE	6.1×10^{-1}	7.8×10^{-2}	4.3×10^{-2}	4.0×10^{-2}	3.9×10^{-2}	$\mathbf{3.3\times 10^{-2}}$
	$ITAE$	5.8×10^{-1}	6.5×10^{-2}	3.9×10^{-2}	3.6×10^{-2}	3.32×10^{-2}	$\mathbf{2.9\times 10^{-2}}$
	ISE	7.6×10^{-2}	8.85×10^{-3}	2.2×10^{-3}	1.9×10^{-3}	1.7×10^{-3}	$\mathbf{1.1\times 10^{-3}}$
	$ITSE$	8.1×10^{-3}	9.3×10^{-4}	4.1×10^{-4}	3.7×10^{-4}	3.4×10^{-4}	$\mathbf{3.1\times 10^{-4}}$
ΔF_2	IAE	5.65×10^{-1}	7.1×10^{-2}	3.9×10^{-2}	3.8×10^{-2}	3.6×10^{-2}	$\mathbf{2.95\times 10^{-2}}$
	$ITAE$	5.23×10^{-1}	5.8×10^{-2}	3.74×10^{-2}	3.3×10^{-2}	3.12×10^{-2}	$\mathbf{2.65\times 10^{-2}}$
	ISE	6.23×10^{-2}	6.25×10^{-3}	1.9×10^{-3}	1.6×10^{-3}	1.3×10^{-3}	$\mathbf{8.21\times 10^{-4}}$
	$ITSE$	7.43×10^{-3}	7.54×10^{-4}	3.8×10^{-4}	3.3×10^{-4}	2.3×10^{-4}	$\mathbf{2.3\times 10^{-4}}$
$\Delta Ptie$	IAE	5.28×10^{-1}	6.85×10^{-2}	3.25×10^{-2}	2.65×10^{-2}	3.55×10^{-2}	$\mathbf{2.85\times 10^{-2}}$
	$ITAE$	4.91×10^{-1}	5.61×10^{-2}	3.54×10^{-2}	2.81×10^{-2}	2.91×10^{-2}	$\mathbf{2.54\times 10^{-2}}$
	ISE	5.96×10^{-2}	5.89×10^{-3}	1.81×10^{-3}	1.35×10^{-3}	1.25×10^{-3}	$\mathbf{7.86\times 10^{-4}}$
	$ITSE$	7.13×10^{-3}	7.21×10^{-4}	3.6×10^{-4}	2.86×10^{-4}	2.12×10^{-4}	$\mathbf{2.23\times 10^{-4}}$

Table 3: Comparative analysis of different control schemes for SLP of 20% in area-1 and SLP of 10% in area-2

SLP of 20% in area-1 and SLP of 10% in area-2							
Performance Indices		**MBA: PID**	**GWO: PID**	**MGWO: PI-PD [14]**	**WHO: FOPID**	**BWOA: FOPD-(1+FOI)**	**WHO: FOPD-(1+FOI)**
OS	ΔF_1(Hz)	0.110	0.0800	0.0600	0.0420	0.0130	**0.0065**
	ΔF_2(Hz)	0.024	0.0130	0.0065	0.0170	0.0013	**0.0008**
	$\Delta Ptie$(puMW)	0.009	0.0055	0.0028	0.0015	0.0005	**0.0002**
US	ΔF_1(Hz)	0.090	0.0750	0.0610	0.0500	0.0130	**0.0065**
	ΔF_2(Hz)	0.028	0.0220	0.0180	0.0140	0.0036	**0.0018**
	$\Delta Ptie$(puMW)	0.011	0.0090	0.0070	0.0057	0.0014	**0.0006**
t_r (sec.)	ΔF_1	0.480	0.4600	0.4200	0.3800	0.4200	**0.4200**

	ΔF_2	0.700	0.7200	0.7000	0.6500	0.7000	**0.7000**
	$\Delta Ptie$	0.700	0.6800	0.6600	0.5800	0.6600	**0.6600**
t_s **(sec.)**	ΔF_1	2.400	2.0000	1.9000	1.8000	1.3000	**1.2000**
	ΔF_2	2.600	2.5000	2.3000	2.4000	2.2000	**2.0000**
	$\Delta Ptie$	3.200	2.7000	2.4000	2.2000	2.0000	**2.0000**
ΔF_1	*IAE*	6.1×10^{-1}	7.8×10^{-2}	4.3×10^{-2}	4.0×10^{-2}	3.9×10^{-2}	$\mathbf{3.3\times 10^{-2}}$
	ITAE	5.8×10^{-1}	6.5×10^{-2}	3.9×10^{-2}	3.6×10^{-2}	3.32×10^{-2}	$\mathbf{2.9\times 10^{-2}}$
	ISE	7.6×10^{-2}	8.85×10^{-3}	2.2×10^{-3}	1.9×10^{-3}	1.7×10^{-3}	$\mathbf{1.1\times 10^{-3}}$
	ITSE	8.1×10^{-3}	9.3×10^{-4}	4.1×10^{-4}	3.7×10^{-4}	3.4×10^{-4}	$\mathbf{3.1\times 10^{-4}}$
ΔF_2	*IAE*	5.65×10^{-1}	7.1×10^{-2}	3.9×10^{-2}	3.8×10^{-2}	3.6×10^{-2}	$\mathbf{2.95\times 10^{-2}}$
	ITAE	5.23×10^{-1}	5.8×10^{-2}	3.74×10^{-2}	3.3×10^{-2}	3.12×10^{-2}	$\mathbf{2.65\times 10^{-2}}$
	ISE	6.23×10^{-2}	6.25×10^{-3}	1.9×10^{-3}	1.6×10^{-3}	1.3×10^{-3}	$\mathbf{8.21\times 10^{-4}}$
	ITSE	7.43×10^{-3}	7.54×10^{-4}	3.8×10^{-4}	3.3×10^{-4}	2.3×10^{-4}	$\mathbf{2.3\times 10^{-4}}$
$\Delta Ptie$	*IAE*	5.28×10^{-1}	6.85×10^{-2}	3.25×10^{-2}	2.65×10^{-2}	3.55×10^{-2}	$\mathbf{2.85\times 10^{-2}}$
	ITAE	4.91×10^{-1}	5.61×10^{-2}	3.54×10^{-2}	2.81×10^{-2}	2.91×10^{-2}	$\mathbf{2.54\times 10^{-2}}$
	ISE	5.96×10^{-2}	5.89×10^{-3}	1.81×10^{-3}	1.35×10^{-3}	1.25×10^{-3}	$\mathbf{7.86\times 10^{-4}}$
	ITSE	7.13×10^{-3}	7.21×10^{-4}	3.6×10^{-4}	2.86×10^{-4}	2.12×10^{-4}	$\mathbf{2.23\times 10^{-4}}$

5.3 Robustness Analysis

In this section, the robustness analysis of the proposed WHO:FOPD-(1+FOI) controller under parametric uncertainties is evaluated. In the practical system, parametric uncertainties may occur in the governor, turbine, reheater, frequency biasing, and governor regulation for both area-1 and area-2 also there will be communication delay in the physical response of all connected elements. The above-mentioned uncertainties will greatly affect the performance of PS; hence a huge number of uncertainties are considered only in the parameters of PS of area-1 (T_{PS1} and K_{PS1}) with SLP of 13% in area-1 and the responses of the proposed controller are depicted in Figs. 9(a)-(c), and 10(a)-(c) with vivid analysis tabulated in Table 4. Firstly, the uncertainties in T_{PS1} as $T_{PS1}/4$ and $4 \times T_{PS1}$ are considered and responses of ΔF_1, ΔF_2 and $\Delta Ptie$ with respect to nominal values are depicted in Figs. 9 (a)-(c) respectively.

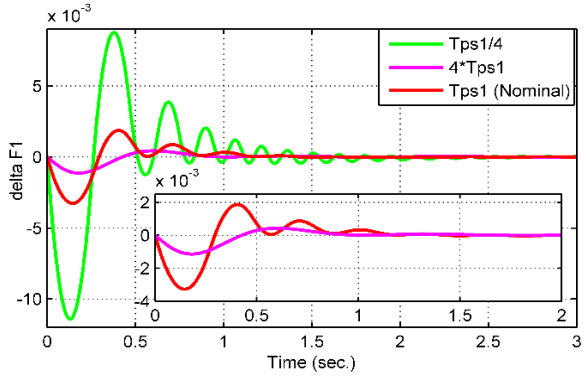

(a)

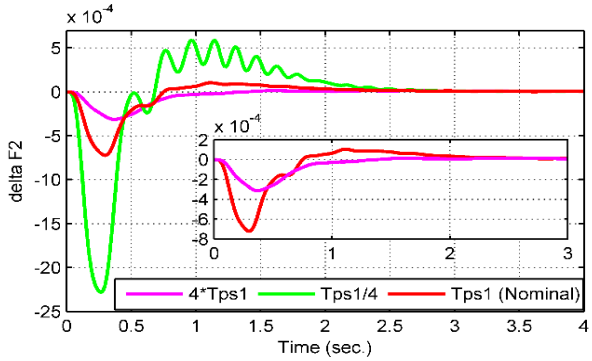

(b)

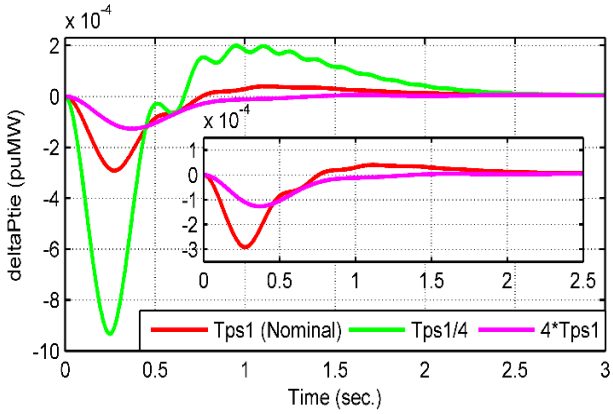

(c)

Fig. 9 Robustness analysis of proposed controller with SLP of 13% in area-1 (a) ΔF_1 (Hz) (b) ΔF_2 (Hz), and (c) $\Delta Ptie$

The maximum OS (0.0097) and US (0.0135) are obtained in ΔF_1 while considering $T_{PS1}/4$. The values of t_s are 2.6 sec., 2.5 sec., and 2.3 sec. are noted for ΔF_1, ΔF_2 and $\Delta Ptie$ respectively for $T_{PS1}/4$. The impact of $4 \times T_{PS1}$ is almost negligible on the performance of the controller as analyzed in Table 4. Moreover, the other uncertainties in K_{PS1} as $3 \times K_{PS1}$ and $K_{PS1}/3$ are considered, and the controller performance is revealed in Figs. 10(a)-(c) and Table 4. The maximum OS (0.0083) and US (0.0092) are obtained in ΔF_1 while considering $3 \times K_{PS1}$ with t_s values are 2.1 sec., 3.1 sec., and 2.3 sec. in ΔF_1, ΔF_2 and $\Delta Ptie$, respectively. The overall effect of $K_{PS1}/3$ is almost negligible as noted in Table 4.

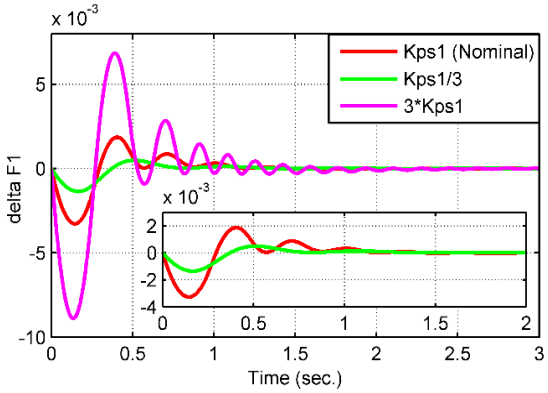

(a)

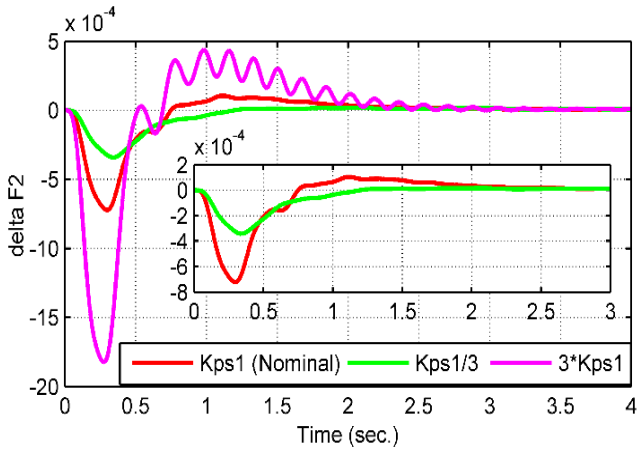

(b)

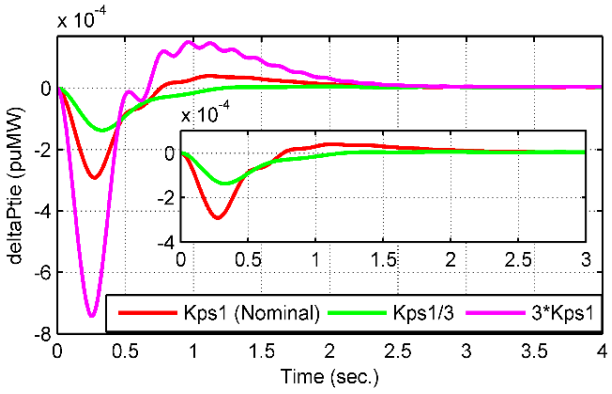

(c)

Fig. 10 Robustness analysis of proposed controller with SLP of 13% in area-1 (a) ΔF_1 (Hz) (b) ΔF_2 (Hz) (c) $\Delta Ptie$

Table 4: Robustness analysis of proposed controller

Proposed controller performance under parametric uncertainties with SLP of 13% in area-1												
Parameters	OS			US			t_r (sec.)			t_s (sec.)		
	ΔF_1(Hz)	ΔF_2(Hz)	$\Delta Ptie$(puMW)	ΔF_1(Hz)	ΔF_2(Hz)	$\Delta Ptie$(puMW)	ΔF_1	ΔF_2	$\Delta Ptie$	ΔF_1	ΔF_2	$\Delta Ptie$
Nominal K_{PS1}, T_{PS1}	0.002	0.00011	Negligible	0.0031	0.00072	0.0003	0.27	0.75	1	1.5	1.9	1
4*T_{PS1}	Negligible	Negligible	Negligible	0.00017	0.00032	0.00012	0.81	1.2	0.91	1	1.2	0.91
T_{PS1}/4	0.0097	0.00064	0.0002	0.0135	0.0023	0.00098	0.25	0.5	0.68	2.6	2.5	2.3
3*K_{PS1}	0.0083	0.00049	0.0002	0.0092	0.0018	0.00093	0.28	0.5	0.62	2.1	3.1	2.3
K_{PS1}/3	Negligible	Negligible	Negligible	0.0018	0.00039	0.00018	0.75	1.3	1.2	0.75	1.3	1.2

5.4 Stability Analysis via Eigenvalue Approach

In order to enhance the dynamic performance of an AGC system, it is necessary to have enough degree of stability. For the purpose of stability evaluation, various methods are available, and eigenvalue is one of them. Before evaluating the eigenvalues, fractional-order terms are converted into their corresponding full-order terms via the SBL method. To show the stability of the proposed controller, the eigenvalues of interconnected two-area PS with WHO-tuned FOPD-(1+FOI) controller are calculated and tabulated in Table 5.

Table 5: Eigenvalues for area-1 and area-2

Area-1	Area-2
$0.0000 + 0.0000i$	$0.0000 + 0.0000i$
$-4.5032 + 47.1896i$	$-5.1691 + 43.2310i$
$-4.5032 - 47.1896i$	$-5.1691 - 43.2310i$
$-12.5000 + 0.0000i$	$-12.5000 + 0.0000i$
$-12.5000 + 0.0000i$	$-12.5000 - 0.0000i$
$-3.6374 + 0.0000i$	$-3.7823 + 0.0000i$
$-3.3333 + 0.0000i$	$-3.3333 + 0.0000i$
$-3.3333 - 0.0000i$	$-3.3333 - 0.0000i$
$-2.1923 + 0.0000i$	$-2.4087 + 0.0000i$
$-1.2608 + 0.0000i$	$-2.0635 + 0.0000i$
$-1.1381 + 0.0000i$	$-1.2734 + 0.0000i$
$-0.8615 + 0.0000i$	$-0.3375 + 0.0000i$
$-0.2001 + 0.0000i$	$-0.3005 + 0.0000i$
$-0.1836 + 0.0000i$	$-0.1989 + 0.0000i$
$-0.1531 + 0.0000i$	$-0.1000 + 0.0000i$
$-0.1000 + 0.0000i$	$-0.1000 - 0.0000i$
$-0.1000 - 0.0000i$	$-0.0558 + 0.0000i$
$-0.0500 + 0.0000i$	$-0.0501 + 0.0000i$
$-0.0500 + 0.0000i$	$-0.0500 + 0.0000i$
$-0.0500 - 0.0000i$	$-0.0500 - 0.0000i$
$-0.0285 + 0.0000i$	$-0.0487 + 0.0000i$
$-0.0228 + 0.0000i$	$-0.0072 + 0.0000i$
$-0.0007 + 0.0000i$	$-0.0060 + 0.0000i$

The TF of outer and inner loop controllers for area-1 and area-2 are revealed by Equations (34)-(37).

$$C_{o,1}(s) = 85.675 + 39.829s^{0.994} \cong 85.675 + 39.829s \quad (34)$$

$$C_{i,1}(s) = 1 + \frac{3.1786}{s^{0.912}} \cong 1 + \frac{3.1786}{s^{0.9}} \quad (35)$$

$$C_{o,2}(s) = 52.909 + 14.845s^{0.987} \cong 52.909 + 14.845s \quad (36)$$

$$C_{i,2}(s) = 1 + \frac{1.88296}{s^{0.1374}} \cong 1 + \frac{1.88296}{s^{0.1}} \quad (37)$$

where $s^{0.9} = \frac{242800s^4+328000s^3+60120s^2+1488s+1}{6648s^4+277300s^3+300600s^2+45610s+887.3}$ and $s^{0.1} = \frac{5532s^4+13380s^3+4147s^2+191.5s+1}{4392s^4+13530s^3+5063s^2+284.5s+1.894}$.

It is clearly noted from Table 5 that all the poles of area-1 and area-2 are present in the left half of s-plane. Hence it is concluded that the proposed WHO:FOPD-(1+FOI) cascade controller is able to stabilize the studied interconnected PS system.

5.5 Real Power System Validation

To benchmark the effectiveness of the proposed WHO: FOPD-(1+FOI) controller, a real New England IEEE-39 test bus system is considered, as shown in Fig. 11. Ten reheat-type thermal generating units are present in the standard IEEE-39 bus system and segregated into three areas [3], [45]. For the validation purpose, only two areas, i.e., area-1 and area-2 are considered. The parameters of the IEEE-39 test bus system are presented in Table 6. The generating units of the same area can be replaced by its equivalent single generation unit with equivalent inertia constant (H_e) and speed regulation (R_e) as follows [3, 5]:

$$H_e = \frac{H_1S_1+H_2S_2+\cdots+H_nS_n}{S_{sys}} \quad (38)$$

$$R_e = \frac{1}{\frac{1}{R_1}\left(\frac{S_1}{S_{sys}}\right)+\frac{1}{R_2}\left(\frac{S_2}{S_{sys}}\right)+\cdots\frac{1}{R_n}\left(\frac{S_n}{S_{sys}}\right)} \text{Hz/MW}_{\text{pu}} \quad (39)$$

and $S_{sys} = S_1 + S_2 + \cdots + S_n$ (40)

where, H_i, R_i and S_i are the individual, inertia constant, speed regulation, and machine rating of the i^{th} generating element and G_{U1} to G_{U10} are the generator unit 1 to 10 in all three areas.

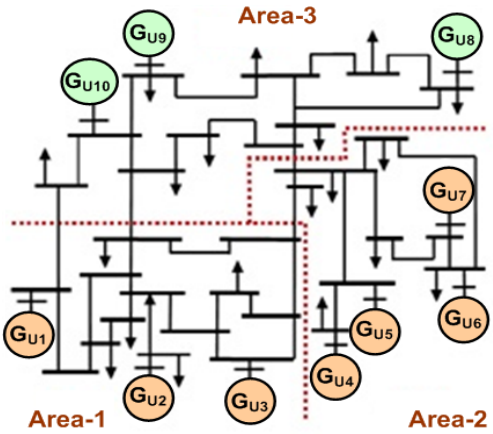

Fig. 11 New England IEEE-39 bus [3], [45]

Table 6: IEEE-39 test bus system parameters [3,5]

Area No.	Unit No.	H	R_d (Hz/MW$_{pu}$)	D (MW$_{pu}$/Hz)	T_g (s)	T_t (s)
1	G_{U1}	4.0	3.0	8.33×10^{-3}	0.08	0.3
	G_{U2}	3.5	3.0	8.33×10^{-3}	0.08	0.3
	G_{U3}	2.5	1.8	8.33×10^{-3}	0.08	0.3
2	G_{U4}	2.5	2.4	8.33×10^{-3}	0.08	0.3
	G_{U5}	3.0	1.8	8.33×10^{-3}	0.08	0.3
	G_{U6}	4.0	2.1	8.33×10^{-3}	0.08	0.3
	G_{U7}	3.0	1.8	8.33×10^{-3}	0.08	0.3
$\alpha_{12} = -1, \beta_1 = \beta_2 = 0.425 Hz/MW_{p.u.}, 2\pi T_{12} = 0.545$puMW/Hz						

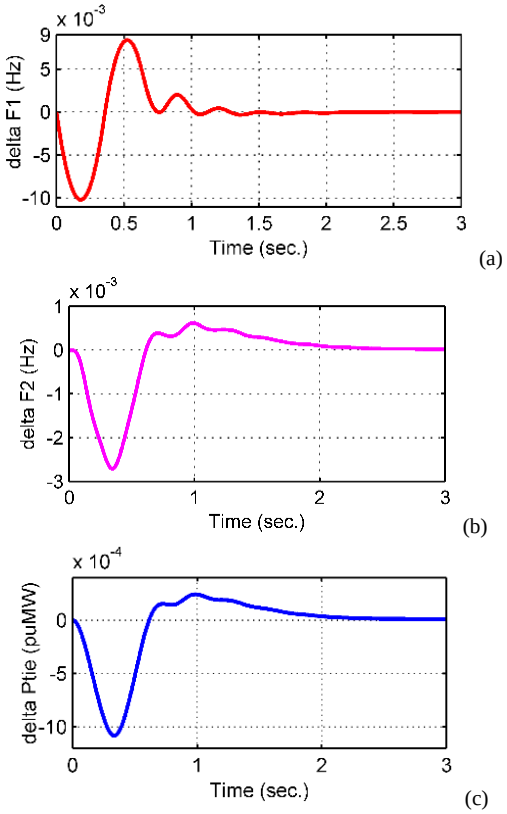

Fig. 12 Controller response for IEEE-39 bus system (a) ΔF_1 (Hz), (b) ΔF_2 (Hz), and (c) $\Delta Ptie$

The proposed controller performance with SLP of 10% in area-1 is shown in Fig. 12. The maximum OS and US in area-1 are 0.0089 Hz and 0.010 Hz, with t_s of 1.3 sec., while dealing with area-2 and tie-line flow, the maximum USs are 0.0029 Hz and 0.0011 puMW with values of t_s are 2.1 sec. and 2 sec. respectively. A vivid comparative analysis of the proposed FOPD-(1+FOI) controller on the simulated and real-time platform is revealed in Table 7.

Table 7: Comparative analysis of proposed controller

SLP of 10% in area-1			
Indices		Simulated	Real-time
OS	ΔF_1(Hz)	0.00230	0.00880
	ΔF_2(Hz)	0.00024	0.00004
	$\Delta Ptie$(puMW)	0.00010	0.00014
US	ΔF_1(Hz)	0.00290	0.01000
	ΔF_2(Hz)	0.00080	0.00270
	$\Delta Ptie$(puMW)	0.00035	0.00110
Rise time (t_r) (sec.)	ΔF_1	0.4000	0.4100
	ΔF_2	0.6500	0.6700
	$\Delta Ptie$	0.6200	0.6700
Settling time (t_s) (sec.)	ΔF_1	1.3000	1.4500
	ΔF_2	1.9000	1.9200
	$\Delta Ptie$	1.9000	1.9200
ΔF_1	IAE	3.3×10^{-2}	4.6×10^{-2}
	$ITAE$	2.9×10^{-2}	4.1×10^{-2}
	ISE	1.1×10^{-3}	2.5×10^{-3}
	$ITSE$	3.1×10^{-4}	4.8×10^{-4}
ΔF_2	IAE	2.95×10^{-2}	4.45×10^{-2}
	$ITAE$	2.65×10^{-2}	4.31×10^{-2}
	ISE	8.21×10^{-4}	8.96×10^{-4}
	$ITSE$	2.3×10^{-4}	2.92×10^{-4}
$\Delta Ptie$	IAE	2.85×10^{-2}	3.48×10^{-2}
	$ITAE$	2.54×10^{-2}	2.94×10^{-2}
	ISE	7.86×10^{-4}	8.93×10^{-4}
	$ITSE$	2.23×10^{-4}	2.65×10^{-4}

6. Conclusion

In this work first time, a novel configuration of WHO-assisted FOPD-(1+FOI) fractional cascade controller is implemented for the load frequency management of an interconnected reheat-type thermal power system network. In the modeling, various non-linearities such as GDB and GRC are considered to replicate the practical scenarios. This controller has the property of both a fractional-order type controller as well as a cascade-type controller. The performance of the proposed controller has been analyzed over five state-of-the-art metaheuristics as MBA, GWO, MGWO, BWOA, and WHO, with four different types of controllers such as PID, PI-PD, FOPID, and FOPD-(1+FOI) under-considered step load perturbations. The obtained results reveal the superiority of the proposed controller in terms of obtained best score (minimization of the objective function), computational cost, speed of convergence, transient response, steady-state response, and considered error rates. While considering the robustness evaluation under practical scenarios of the proposed controller, the performance of the controller is quite satisfactory with lesser

OS and US, and faster settling time. The stability analysis of the proposed scheme is successfully evaluated via the eigenvalue approach. Finally, to benchmark, the performance of the proposed controller on a real power system, an IEEE-39 New England bus system is implemented successfully, and the comparative tabular analysis of simulated and real power system analysis shows satisfactory performance. The future scope of this work will predominately focus on the controller design for interconnected power systems under high renewable penetrations.

7. References

[1] M. Ramesh, A. K. Yadav, and P. K. Pathak, "An extensive review on load frequency control of solar-wind based hybrid renewable energy systems," *Energy Sources, Part A: Recovery, Utilization, and Environmental Effects*, pp. 1-25, 2021.

[2] M. Kumar and Y. V. Hote, "Robust PIDD2 controller design for perturbed load frequency control of an interconnected time-delayed power systems," *IEEE Transactions on Control Systems Technology*, vol. 29, no. 6, pp. 2662-2669, 2021.

[3] N. Pathak and Z. Hu, "Hybrid-peak-area-based performance index criteria for AGC of multi-area power systems," *IEEE Transactions on Industrial Informatics*, vol. 15, no. 11, pp. 5792-5802, 2019.

[4] N. Pathak, T. Bhatti, A. Verma, and I. Nasiruddin, "AGC of two area power system based on different power output control strategies of thermal power generation," *IEEE Transactions on Power Systems*, vol. 33, no. 2, pp. 2040-2052, 2017.

[5] M. Ramesh, A. K. Yadav, and P. K. Pathak, "Intelligent adaptive LFC via power flow management of integrated standalone micro-grid system," *ISA transactions*, vol. 112, pp. 234-250, 2021.

[6] Y. Arya, "ICA assisted FTIλDN controller for AGC performance enrichment of interconnected reheat thermal power systems," *Journal of Ambient Intelligence and Humanized Computing*, pp. 1-17, 2021.

[7] M. H. Cintuglu and O. A. Mohammed, "Behavior modeling and auction architecture of networked microgrids for frequency support," *IEEE Transactions on Industrial Informatics*, vol. 13, no. 4, pp. 1772-1782, 2016.

[8] Y. Arya and N. Kumar, "BFOA-scaled fractional order fuzzy PID controller applied to AGC of multi-area multi-source electric power generating systems," *Swarm and Evolutionary Computation*, vol. 32, pp. 202-218, 2017.

[9] R. Patel, C. Li, L. Meegahapola, B. McGrath, and X. Yu, "Enhancing optimal automatic generation control in a multi-area power system with diverse energy resources," *IEEE Transactions on Power Systems*, vol. 34, no. 5, pp. 3465-3475, 2019.

[10] S. Panda, B. Mohanty, and P. K. Hota, "Hybrid BFOA–PSO algorithm for automatic generation control of linear and nonlinear interconnected power systems," *Applied soft computing*, vol. 13, no. 12, pp. 4718-4730, 2013.

[11] E. S. Ali and S. M. Abd-Elazim, "Bacteria foraging optimization algorithm based load frequency controller for interconnected power system," *International Journal of Electrical Power & Energy Systems*, vol. 33, no. 3, pp. 633-638, 2011.

[12] S. M. Abd-Elazim and E. S. Ali, "Load frequency controller design of a two-area system composing of PV grid and thermal generator via firefly algorithm," *Neural Computing and Applications*, vol. 30, no. 2, pp. 607-616, 2018.

[13] M. Farahani, S. Ganjefar, and M. Alizadeh, "PID controller adjustment using chaotic optimisation algorithm for multi-area load frequency control," *IET Control Theory & Applications*, vol. 6, no. 13, pp. 1984-1992, 2012.

[14] S. Padhy, S. Panda, and S. Mahapatra, "A modified GWO technique based cascade PI-PD controller for AGC of power systems in presence of plug in electric vehicles," *Engineering Science and Technology, an International Journal*, vol. 20, no. 2, pp. 427-442, 2017.

[15] M. Omar, M. Soliman, A. A. Ghany, and F. Bendary, "Optimal tuning of PID controllers for hydrothermal load frequency control using ant colony optimization," *International journal on electrical engineering and informatics*, vol. 5, no. 3, p. 348, 2013.

[16] C. K. Shiva, G. Shankar, and V. Mukherjee, "Automatic generation control of power system using a novel quasi-oppositional harmony search algorithm," *International Journal of Electrical Power & Energy Systems*, vol. 73, pp. 787-804, 2015.

[17] P. K. Pathak, S. Padmanaban, A. K. Yadav, P. A. Alvi, and B. Khan, "Modified incremental conductance MPPT algorithm for SPV-based grid-tied and stand-alone systems," *IET Generation, Transmission & Distribution*, vol. *16*, no. 4, pp. 776-791, 2022.

[18] D. Guha, P. K. Roy, and S. Banerjee, "Study of differential search algorithm based automatic generation control of an interconnected thermal-thermal system with governor dead-band," *Applied Soft Computing*, vol. 52, pp. 160-175, 2017.

[19] P. Hota and B. Mohanty, "Automatic generation control of multi source power generation under deregulated environment," *International Journal of Electrical Power & Energy Systems*, vol. 75, pp. 205-214, 2016.

[20] H. M. Hasanien and A. A. El-Fergany, "Symbiotic organisms search algorithm for automatic generation control of interconnected power systems including wind farms," *IET Generation, Transmission & Distribution*, vol. 11, no. 7, pp. 1692-1700, 2017.

[21] H. Gozde, M. C. Taplamacioglu, and I. Kocaarslan, "Comparative performance analysis of Artificial Bee Colony algorithm in automatic generation control for interconnected reheat thermal power system," *International Journal of Electrical Power & Energy Systems*, vol. 42, no. 1, pp. 167-178, 2012.

[22] D. Guha, P. K. Roy, and S. Banerjee, "Load frequency control of interconnected power system using grey wolf optimization," *Swarm and Evolutionary Computation*, vol. 27, pp. 97-115, 2016.

[23] S. P. Singh, T. Prakash, V. Singh, and M. G. Babu, "Analytic hierarchy process based automatic generation control of multi-area interconnected power system using Jaya algorithm," *Engineering applications of artificial intelligence*, vol. 60, pp. 35-44, 2017.

[24] A. D. Rosaline and U. Somarajan, "Structured H-Infinity controller for an uncertain deregulated power system," *IEEE Transactions on Industry Applications*, vol. 55, no. 1, pp. 892-906, 2018.

[25] K. Vrdoljak, N. Perić, and I. Petrović, "Sliding mode based load-frequency control in power systems," *Electric Power Systems Research*, vol. 80, no. 5, pp. 514-527, 2010.

[26] S. Sondhi and Y. V. Hote, "Fractional order PID controller for load frequency control," *Energy Conversion and Management*, vol. 85, pp. 343-353, 2014.

[27] X. Liu, Y. Zhang, and K. Y. Lee, "Coordinated distributed MPC for load frequency control of power system with wind farms," *IEEE Transactions on Industrial Electronics*, vol. 64, no. 6, pp. 5140-5150, 2016.

[28] A. M. Ersdal, L. Imsland, and K. Uhlen, "Model predictive load-frequency control," *IEEE Transactions on Power Systems*, vol. 31, no. 1, pp. 777-785, 2015.

[29] A. G. Haroun and Y. Li, "A novel optimized hybrid fuzzy logic intelligent PID controller for an interconnected multi-area power system with physical constraints and boiler dynamics," *ISA Transactions*, vol. 71, pp. 364-379, 2017.

[30] D. Sharma and S. Mishra, "Non-linear disturbance observer-based improved frequency and tie-line power control of modern interconnected power systems," *IET Generation, Transmission & Distribution*, vol. 13, no. 16, pp. 3564-3573, 2019.

[31] L. C. Saikia, Sukumar Mishra, Nidul Sinha, and J. Nanda., "Automatic generation control of a multi area hydrothermal system using reinforced learning neural network controller," *International Journal of Electrical Power & Energy Systems*, vol. 33, no. 4, pp. 1101-1108, 2011.

[32] A. Fathy, & Kassem, A. M., "Antlion optimizer-ANFIS load frequency control for multi-interconnected plants comprising photovoltaic and wind turbine," *ISA Transactions*, vol. 87, pp. 282-296, 2019.

[33] A. Latif, S. S. Hussain, D. C. Das, and T. S. Ustun, "Double stage controller optimization for load frequency stabilization in hybrid wind-ocean wave energy based maritime microgrid system," *Applied Energy*, vol. 282, pp. 116171, 2021.

[34] A. A. Abou El-Ela, R. A. El-Sehiemy, A. M. Shaheen, and A. E. G. Diab, "Design of cascaded controller based on coyote optimizer for load frequency control in multi-area power systems with renewable sources," *Control Engineering Practice*, vol. 121, pp. 105058, 2022.

[35] C. Pradhan, and C. N. Bhende, "Online load frequency control in wind integrated power systems using modified Jaya optimization," *Engineering Applications of Artificial Intelligence*, vol. 77, pp. 212-228, 2019.

[36] E. Çelik, "Performance analysis of SSA optimized fuzzy 1PD-PI controller on AGC of renewable energy assisted thermal and hydro-thermal power systems," *Journal of Ambient Intelligence and Humanized Computing*, pp. 1-20, 2022.

[37] M. Sharma, S. Dhundhara, Y. Arya, and S. Prakash, "Frequency excursion mitigation strategy using a novel COA optimised fuzzy controller in wind integrated power systems," *IET Renewable Power Generation*, vol. 14, no. 19, pp. 4071-85, 2020.

[38] A. Abazari, H. Monsef, B. Wu, "Coordination strategies of distributed energy resources including FESS, DEG, FC and WTG in load frequency control (LFC) scheme of hybrid isolated micro-grid," *International Journal of Electrical Power & Energy Systems*, vol. 109, pp. 535-547, 2019.

[39] E. Çelik, Öztürk, N., Arya, Y., & Ocak, C., "(1+ PD)-PID cascade controller design for performance betterment of load frequency control in diverse electric power systems " *Neural Computing and Applications*, pp. 1-24, 2021.

[40] P. K. Pathak, A. K. Yadav, A. Shastri & P.A. Alvi, "BWOA assisted PIDF-(1+ I) controller for intelligent load frequency management of standalone micro-grid," *ISA Transactions*, pp. 1-15, 2022. https://doi.org/10.1016/j.isatra.2022.06.010

[41] P. Dash, Saikia, L. C., & Sinha, N. , "Automatic generation control of multi area thermal system using Bat algorithm optimized PD–PID cascade controller," *International Journal of Electrical Power & Energy Systems*, vol. 68, pp. 364-372, 2015.

[42] R. Sivalingam, Chinnamuthu, S., & Dash, S. S., "A hybrid stochastic fractal search and local unimodal sampling based multistage PDF plus (1+ PI) controller for automatic generation control of power systems," *Journal of the Franklin Institute* vol. 354, no. 12, pp. 4762-4783., 2017.

[43] I. Naruei, & Keynia, F., "Wild horse optimizer: a new meta-heuristic algorithm for solving engineering optimization problems. Engineering with Computers," pp. 1-32, 2021.

[44] V. Hayyolalam, & Kazem, A. A. P., "Black widow optimization algorithm: a novel meta-heuristic approach for solving engineering optimization problems," *Engineering Applications of Artificial Intelligence,*, vol. 87, p. 103249, 2020.

[45] S. Jain and Y. V. Hote, "Design of generalised active disturbance rejection control for delayed systems: an application to load frequency control," *International Journal of Control*, vol. 94, no. 11, pp. 3146-3160, 2021.

[46] J. Morsali, K. Zare, and M. T. Hagh, "Applying fractional order PID to design TCSC-based damping controller in coordination with automatic generation control of interconnected multi-source power system," *Engineering Science and Technology, an International Journal*, vol. 20, no. 1, pp. 1-17, 2017.

[47] I. Pan, and S. Das, "Fractional order AGC for distributed energy resources using robust optimization," *IEEE Transactions on smart grid*, vol. 7, no. 5, pp. 2175-2186, 2015.

[48] F. N. Deniz, B. B. Alagoz, N. Tan, and D. P. Atherton, "An integer order approximation method based on stability boundary locus for fractional order derivative/integrator operators," *ISA Transactions*, vol. 62, pp. 154-163, 2016.

Appendix

Parameters of 2-area Reheat Thermal Power System [6]:

$R_i = 2.4$ Hz/puMW, $\beta_i = 0.425$Hz/$MW_{p.u.}$, $T_{Ti} = 0.3$ sec., $T_{Gi} = 0.08$sec., $T_{ri} = 10$ sec., $K_{ri} = 0.5$, $K_{PSi} = 120$Hz/puMW, $T_{PSi} = 20$ sec., $\alpha_{12} = -1$, $2\pi T_{12} = 0.545$ puMW/Hz, where, $i = 1, 2$.